University of Bath

Alternative formats
If you require this document in an alternative format, please contact:
openaccess@bath.ac.uk

Establishing virtual bioequivalence and clinically relevant specifications using *in vitro* biorelevant dissolution testing and physiologically-based population pharmacokinetic modeling. Case example: Naproxen

Authors: Ioannis Loisios-Konstantinidis[1], Rodrigo Cristofoletti[2], Nikoletta Fotaki[3], David B. Turner[5], Jennifer Dressman[1,4]

Author Information:

[1] Institute of Pharmaceutical Technology, Goethe University, Frankfurt am Main, Germany,

[2] Center for Pharmacometrics and Systems Pharmacology, Department of Pharmaceutics, College of Pharmacy, University of Florida, Orlando, Florida, USA.

[3] Department of Pharmacy and Pharmacology, Faculty of Science, University of Bath, Bath, UK,

[4] Fraunhofer IME - Translational Pharmacology and Medicine, Carl-von-Noorden Platz 9, Frankfurt am Main, Germany

[5] Certara UK Limited, Simcyp Division, 1 Concourse Way, Sheffield S1 2BJ, United Kingdom

Correspondence:

Jennifer Dressman, Biocenter, Institute of Pharmaceutical Technology, Johann Wolfgang Goethe University, Max-von-Laue-Str. 9, Frankfurt am Main 60438, Germany. Email: dressman@em.uni-frankfurt.de

Abstract:

Background: Physiologically-based population pharmacokinetic modeling (popPBPK) coupled with *in vitro* biopharmaceutics tools such as biorelevant dissolution testing can serve as a powerful tool to establish virtual bioequivalence and set clinically relevant specifications. One of several applications of popPBPK modeling is in the emerging field of virtual bioequivalence (VBE), where it can be used to streamline drug development by implementing model-informed formulation design and to inform regulatory decision-making e.g., with respect to evaluating the possibility of extending BCS-based biowaivers beyond BCS Class I and III compounds in certain cases.

Methods: In this study, Naproxen, a BCS class II weak acid was chosen as the model compound. *In vitro* biorelevant solubility and dissolution experiments were performed and the resulting data were used as an input to the PBPK model, following a stepwise workflow for the confirmation of the biopharmaceutical parameters. The naproxen PBPK model was developed by implementing a middle-out approach and verified against clinical data obtained from the literature. Once confidence in the performance of the model was achieved, several *in vivo* dissolution scenarios, based on model-based analysis of the *in vitro* data, were used to simulate clinical trials in healthy adults. Inter-occasion variability (IOV) was also added to critical *physiological* parameters and mechanistically propagated through the simulations. The various trials were simulated on a "worst/best case" dissolution scenario and average bioequivalence was assessed according to C_{max}, AUC and t_{max}.

Results: VBE results demonstrated that naproxen products with *in vitro* dissolution reaching 85% dissolved within 90 minutes would lie comfortably within the bioequivalence limits for C_{max} and AUC. Based on the establishment of VBE, a dissolution "safe space" was designed and a clinically relevant specification for naproxen products was proposed. The interplay between formulation-related and drug-specific PK parameters (e.g., t1/2) to predict the *in vivo* performance was also investigated.

Conclusion: Over a wide range of values, the *in vitro* dissolution rate is not critical for the clinical performance of naproxen products and therefore naproxen could be eligible for BCS-based biowaivers

47 based on *in vitro* dissolution under intestinal conditions. This approach may also be applicable to other

48 poorly soluble acidic compounds with long half-lives, providing an opportunity to streamline drug

49 development and regulatory decision-making without putting the patient at a risk.

50

51 **Key words**: PBPK, modeling & simulation; virtual bioequivalence; IVIVE, clinically relevant

52 specifications; dissolution safe-space; biorelevant dissolution

53

Table of Contents

89

90

91

1 Introduction

93

Physiologically-based population pharmacokinetic (popPBPK) modelling has been implemented successfully to support and inform drug product development and regulatory decision-making.(Babiskin and Zhang, 2015; Doki et al., 2017; Heimbach et al., n.d.; Mitra, 2019; Olivares-Morales et al., 2016; Parrott et al., 2014; Pepin et al., 2016; Stillhart et al., 2017; Suarez-Sharp et al., 2018; Zhang et al., 2017) Patient-centric, model-informed drug product development necessitates an *in vitro-in vivo-in silico* link to establish clinically relevant specifications and thus guarantee the quality of the drug product with respect to safety and efficacy. By encompassing model-informed formulation selection and prediction of clinical performance, modeling and simulation (M & S) provides a way forward to the design of "safe spaces", and thus offer regulatory relief. Some examples include guiding development of biorelevant and/or biopredictive dissolution methods to support biowaiver extensions and enabling extrapolation to special populations (e.g., paediatrics). Although the current PBPK regulatory guidelines still mainly focus on the prediction of drug-drug interactions (DDIs),(European Medicines Agency (EMA), 2018a; U.S.FDA Center for Drug Evaluation and Research (CDER), 2018a) the integration of translational biopharmaceutical modeling and dissolution testing has been attracting increased attention from leading pharmaceutical industries as well as regulatory bodies and over the last few years, the regulatory impact of mechanistic absorption modeling has significantly increased.(Babiskin and Zhang, 2015; Heimbach et al., 2019; Pepin et al., 2016; Zhang et al., 2017)

Establishing bioequivalence (BE) has been a critical component of and remains a challenge during development of both new drug and generic products. In the context of quality by design (QbD) and the biopharmaceutics risk assessment roadmap (BioRAM),(Selen et al., 2014),(Dickinson et al., 2008) the importance of linking *in vitro* with *in vivo* data bi-directionally has received greater emphasis. Accordingly, virtual bioequivalence (VBE) can serve as a powerful tool to set clinically relevant

116   specifications and predict anticipated clinical outcomes in healthy, patient and special-patient (e.g.,

117   paediatrics and/ or co-administration of PPIs) populations. To accurately predict the *in vivo*

118   performance of a drug product through clinical trial simulation, a certain set of conditions needs to be

119   met. This includes integration of biorelevant *in vitro* data into the simulation model as well as

120   mechanistic absorption modelling, disposition/elimination components and consideration of

121   physiological and physicochemical interactions with the formulation. After developing the mechanistic

122   absorption PBPK model, it must be verified via learn/ confirm cycles which rely on evaluation against

123   observed clinical data. Such models can then be used to predict the population pharmacokinetic

124   variability of the test drug/ formulation and therefore enable assessment of bioequivalence risks via

125   virtual trials simulations.(Pathak et al., 1997)

126   The ability of PBPK to account for between-subject (BS), within-subject (WS) and inter-occasion

127   variability (IOV) is crucial to the accuracy and the applicability of VBE results. Although the current

128   techniques can address the between-subject variability reasonably well, progress still needs to be

129   made in the area of estimating inter-occasion variability. Two independent modeling strategies to

130   incorporate IOV in VBE studies have been implemented in the literature: a) *a priori* estimated random

131   error terms in replicate clinical study are added to the PK parameters, or, more mechanistically, b) the

132   IOV is integrated into the system parameters and propagated in simulations.(Wedagedera et al., 2017)

133   In this study, an *in vitro-in vivo-in silico* workflow to establish VBE and clinically relevant dissolution

134   specifications is proposed. Naproxen and its sodium salt was chosen as the case example. Naproxen is

135   a weakly acidic (pK$_a$ ≈4.4) non-steroid anti-inflammatory (NSAID) agent. It is a biopharmaceutical

136   classification system (BCS) class II weak acid with poor solubility in the fasted stomach but freely

137   soluble in the intestinal environment and has a high permeability, similar to ibuprofen and

138   diclofenac.(Cristofoletti et al., 2013; Cristofoletti and Dressman, 2016; Kambayashi et al., 2013) Since

139   the absorption of such compounds is usually complete, they have been identified as offering

140   opportunities for a potential BCS-based biowaiver extension.(Cristofoletti and Dressman, 2016; Tubic-

141   Grozdanis et al., 2008; Yazdanian et al., 2004) The free acid (Naprosyn®) and the sodium salt

142 (Anaprox®) forms are administered orally as immediate release (IR) tablets. The purpose of this article

143 is to characterize the *in vitro* dissolution behavior of naproxen pure API and formulations, integrate

144 mechanistic absorption modeling with population-based PBPK, design a safe space and, last but not

145 least, set clinically relevant dissolution specifications through VBE trials. The possibility/ risk of granting

146 BCS-biowaiver for naproxen products is also investigated.

147

2 Material and Methods

149

2.1 Chemicals and reagents

151

152 Naproxen (lot #SLBV2253) and naproxen sodium (lot #MKCD6021) pure active pharmaceutical

153 ingredient (API) were purchased commercially from Sigma-Aldrich Co., LLC. (St. Louis, MO). Naproxen

154 tablets (500 mg Naprosyn®, lot 70662; Minerva Pharmaceutical Inc., Athens, Greece) and naproxen

155 sodium tablets (550 mg Anaprox®, lot 70466; Minerva Pharmaceutical Inc., Athens, Greece) were

156 commercially purchased from the Greek market. Fasted state simulated gastric fluid (FaSSGF)/fasted

157 state simulated intestinal fluid (FaSSIF V1)/fed state simulated intestinal fluid (FeSSIF V1) powder (lot

158 01-1512-05NP), FeSSIF V2 powder (lot 03-1610-02) and FaSSIF V3 powder (lot PHA S 1306023) were

159 kindly donated from Biorelevant.com Ltd., (Surrey, UK). Acetonitrile (lot 18A101551) and water (lot

160 17B174006) of HPLC-grade were from VWR Chemicals (Leuven, Belgium). Sodium hydroxide pellets

161 (lot 14A100027), sodium chloride (lot 17I074122), sodium acetate (lot 14B240013), hydrochloric acid

162 37% (lot 10L060526), orthophosphoric acid 85% (lot 12K210017) and glacial acetic acid 100% (lot

163 12B220508) were commercially obtained from VWR Chemicals (Leuven, Belgium). Sodium dihydrogen

164 phosphate dehydrate (lot K93701642712), maleic acid (lot 57118880544) and citric acid (lot

165   K91221207425) were commercially purchased from Merck KGaA (Darmstadt, Germany). Pepsin from

166   pocrine gastric mucosa 19.6% and Lipofundin® MCT/LCT 20% were from Sigma-Aldrich Co., LLC. (St.

167   Louis, MO) and B. Braun Melsungen AG (Melsungen, Germany), respectively.

168

169   ## 2.2   *In vitro* solubility experiments

170

171   The solubility of naproxen and its sodium salt was investigated in various selected aqueous and

172   biorelevant dissolution media using the Uniprep™ system (Whatman®, Piscataway, NJ, USA). All

173   aqueous buffers were prepared according to the European Pharmacopoeia, while the biorelevant

174   media were prepared according to Markopoulos et al. and Fuchs et al.(Fuchs et al., 2015; Markopoulos

175   et al., 2015) The composition and physicochemical characteristics of the fasted and fed state

176   biorelevant media used in this study are summarized in Table 1. An excess amount of API was added

177   to 3 mL of dissolution medium and the samples were incubated for 24 h at 37°C on an orbital mixer.

178   The samples were then filtered through the 0.45 µm PTFE filter integrated in the Uniprep™ system.

179   The filtrate was immediately diluted with mobile phase and analyzed by high-performance liquid

180   chromatography (HPLC) (see section 2.5). All measurements were performed at least in triplicate (n≥3).

181

182   *Table 1: Composition and physicochemical characteristics of biorelevant media in the fasted and fed states.*

183

184   ## 2.3   *In vitro* dissolution tests

185

186   All dissolution tests were performed using calibrated USP II (paddle) apparatus (Erweka DT 80,

187   Heusenstamm, Germany) at 37 ± 0.4°C. Each vessel contained 500 mL of fresh, pre-warmed medium

188   and the rotational speed was set at 75 rpm. Samples were withdrawn at 2.5, 5, 10, 15, 20, 30, 45, 60,

189   90 and 120 minutes via a 5 mL glass syringe connected to a stainless-steel cannula containing a 10 μm

190   polyethylene cannula filter. Immediately thereafter, the sample was filtered through a 0.45 μm PTFE

191   filter (ReZist™ 30, GE Healthcare UK Ltd., Buckinghamshire, UK), discarding the first 2 mL. The filtrate

192   was immediately diluted with mobile phase and analyzed by HPLC-UV (see section 2.5). The removal

193   of 5 mL at each sampling time was taken into account in the calculation of the percentage dissolved.

194   All experiments were performed at least in triplicate (n≥3) and the final pH in the vessel was recorded.

195

2.4   Two-stage dissolution tests

197

198   Since the conventional one-stage USP II dissolution test does not include a gastric compartment to

199   account for disintegration of the dosage form in the stomach, differences in the disintegration time

200   between non-coated (i.e. 500 mg Naprosyn®) and simple coated formulation (i.e. 550 mg Anaprox®)

201   might bias the interpretation of the biorelevant *in vitro* dissolution behavior with respect to the *in vivo*

202   performance. Therefore, to investigate the disintegration effect on the *in vitro* performance of

203   naproxen/ naproxen sodium formulations, a two-stage dissolution test for FaSSIF V3 was developed

204   based on the publication by Mann et al. (Mann et al., 2017)

205   The dosage form was initially exposed to 250 mL of FaSSGF Level III and samples were removed at 5,

206   10, 15, 20, 30 minutes and treated as described in section 2.3. After the withdrawal of the last sample,

207   6.8 mL of sodium hydroxide 1M and immediately thereafter 250 mL of FaSSIF V3 concentrate pH=6.7

208   (double concentration of all the constituents, apart from sodium hydroxide) were added to the vessel.

209   Instead of increasing the pH of the intestinal medium concentrate to counterbalance the acidic pH of

210   the stomach medium as described in the original study,(Mann et al., 2017) sodium hydroxide was

211   added first, but almost simultaneously, with the FaSSIF V3 concentrate. This was done to avoid using

212   a very high pH in the FaSSIF V3 concentrate. After addition of sodium hydroxide and concentrated

213 FaSSIF V3, further samples were removed at 32.5, 35, 40, 45, 50, 60 and 90 minutes. The two-stage

214 experiments were performed using calibrated USP II (paddle) apparatus (Erweka DT 80, Heusenstamm,

215 Germany) at 37$\pm$0.4°C and the samples were analyzed by HPLC-UV (see section 2.5). All experiments

216 were performed at least in triplicate (n≥3) and the final pH in the vessel was recorded.

217

218

219 ## 2.5 Quantitative Analysis of Samples

220

221 Samples obtained from solubility and dissolution experiments were first filtered through a 0.45 µm

222 PTFE filter (ReZist™ 30 syringe filter or Uniprep™; Whatman®, Piscataway, NJ, USA) and subsequently,

223 after appropriate dilution with mobile phase, they were analyzed by HPLC-UV (Hitachi Chromaster;

224 Hitachi Ltd., Tokyo, Japan or Spectra System HPLC, ThermoQuest Inc., San Jose, USA). A BDS Hypersil

225 C18, 5 µm, 150 x 4.6 mm (Thermo Scientific) analytical column combined with a pre-column (BDS

226 Hypersil C-18, 3µm, 10 x 4mm) was used. The mobile phase consisted of 20 mM NaH_2PO_4 buffer

227 adjusted to pH=3.0 and acetonitrile (60:40 % v/v). The detection wavelength was set at 273 nm, the

228 flow rate at 1.2 mL/min and the injection volume at 20 µL. Using this method, the retention time was

229 approximately 7.3 minutes. The limit of detection (LOD) and quantification (LOQ) were 0.03 and 0.1

230 µg/mL, respectively.

231 ## 2.6 Model-based analysis of *in vitro* solubility data

232

233 An experimental estimate of the naproxen pK_a was obtained by fitting the Henderson-Hasselbalch

234 equation (Eq. 1) to the mean aqueous equilibrium solubility (S_i) values using the SIVA Toolkit® (n=6;

235 all aqueous buffers). As intrinsic solubility (S_0), the lowest reported value in buffers was used. The pK_a

236   was then compared with values available in the literature to confirm the validity of the aqueous

237   solubility parameter estimates.

$$S_i = S_0 \cdot (10^{\,pH-pKa})$$ (1)

238

239   The impact of bile salt concentration ($[BS]$) and subsequent formation of micelles on the solubility of

240   naproxen was investigated. This was done by mechanistically modelling the mean solubility values in

241   fasted state biorelevant media (n=3), accounting also for the relative proportions of naproxen

242   solubilized in the aqueous versus the micelle phases, using the total solubility $\left(S_{(BS)Tot}\right)$ equation (Eq.

243   2) in SIVA Toolkit® version 3.0 (SIVA; Certara, Simcyp Division; Sheffield, UK). Estimates of the logarithm

244   of the micelle-water partition coefficient for the neutral $\left(K_{m:w,unionized}\right)$ and ionized drug

245    $\left(K_{m:w,ionized}\right)$ were obtained to quantify the micelle-mediated solubility.

$$S_{(BS)Tot} = \left([BS] \cdot \frac{S_0}{C_{H2O}} \cdot K_{m:w,unionized} + S_0 \right) + \left([BS] \cdot \frac{S_i}{C_{H2O}} \cdot K_{m:w,ionized} + S_i \right)$$ (2)

246   Where C_{H2O} stands for the concentration of water.

247   Estimation of the relevant parameters was performed using the Nelder-Mead algorithm and weighting

248   by the reciprocal of the predicted values was chosen. After model verification, all obtained estimates

249   were used as input parameters for the development of the physiologically-based pharmacokinetic

250   model (PBPK) model (see section 2.9)

2.7   Model-based analysis of *in vitro* dissolution data

251

252

253   Once confidence in the estimation of solubility-related parameters was established, further model-

254   based analysis of the *in vitro* dissolution data obtained from both the one and two-stage tests was

255   performed within the serial dilution module of the SIVA Toolkit® (SIVA 3.0). The dissolution rate of

256   spherical particles under sink and non-sink conditions within SIVA is described by an extension of the

257   diffusion layer model (DLM) developed by Wang and Flanagan. (Eq. 3) (Wang and Flanagan, 2002,

258   1999)

$$DR(t) = -N \cdot S_{DLM} \cdot \frac{D_{eff}}{h_{eff}(t)} \cdot 4\pi \cdot \alpha(t) \cdot \left(\alpha(t) + h_{eff}(t)\right) \cdot \left(S_{surface}(t) - C_{bulk}(t)\right) \quad (3)$$

259

260   where $DR(t)$ is the dissolution rate at time *t*; *N* is the number of particles in a given particle size bin;

261   S_{DLM} is a lumped, empirical, correction scalar without regard to the mechanistic origin of the required

262   correction to the DLM. The estimated S_{DLM} values obtained with SIVA can be applied to the Simcyp

263   PBPK simulator to reflect differences between media or formulations; D_{eff} is the effective diffusion

264   coefficient; $h_{eff}(t)$ and $\alpha(t)$ represent the thickness of the hydrodynamic boundary layer and the

265   particle radius at time *t* respectively; $S_{surface}(t)$ corresponds to the saturation solubility at the particle

266   surface (which may be different to the bulk fluid solubility as discussed below); and $C_{bulk}(t)$ is the

267   concentration of dissolved drug in bulk solution at time t.

268   The $h_{eff}(t)$ was calculated by the fluid dynamics sub-model, which enables the hydrodynamic

269   conditions to be described according to local conditions and stirring rate. Fluid dynamics-based $h_{eff}(t)$

270   is the recommended option for describing the hydrodynamics, as it permits a more rational translation

271   of estimated parameters such as the S_{DLM} to *in vivo* conditions, in which the hydrodynamics are

272   usually quite different to *in vitro* experiments.

273   The local pH at the particle surface of ionisable drugs can significantly affect the $S_{surface}$ and

274   consequently the dissolution rate.(K. G. Mooney et al., 1981; K.G. Mooney et al., 1981a, 1981b; Ozturk

275   et al., 1988; Serajuddin and Jarowski, 1985; Sheng et al., 2009) Since in the *in vitro* dissolution media

276   have a somewhat higher buffer capacity than the intestinal fluids, the self-buffering effect at the solid

277   surface can be underestimated. For this reason, the surface pH was calculated and directly input into

278   SIVA. The calculation of the surface pH was based on the model proposed by Mooney et al.(K.G.

279   Mooney et al., 1981a), which assumes that dissolution is the result of both chemical reaction between

280 the conjugate base of the buffer species and the hydrogen cations released from the dissolving drug

281 (in this case naproxen free acid (NPX-H)) the liquid-solid interface and the diffusion of the dissolved

282 particles to the bulk. This model is very similar to the quasi-equilibrium model published by Ozturk et

283 al.(Ozturk et al., 1988), a derivation of which is implemented in SIVA as the default option for surface

284 pH calculations.

285 By fitting the DLM model to the observed dissolution data, accurate S_{DLM} estimates for each

286 dissolution and two-stage test were obtained. In the case of two-stage testing, the gastric and

287 intestinal profiles were treated separately. Under fasted state intestinal conditions, naproxen is freely

288 soluble and therefore *in vitro* dissolution is not expected to be solubility limited. In that case,

289 disintegration of the solid dosage form in the intestinal dissolution medium might be the rate-limiting

290 step for the *in vitro* dissolution rate, especially in single dissolution experiments where the dosage

291 form is directly exposed to the intestinal medium without any pre-treatment with gastric medium to

292 account for disintegration in the stomach. In order to distinguish and model the relative impact of

293 disintegration on the overall dissolution, the first-order disintegration option was activated in SIVA and

294 used to obtain estimates of the first-order disintegration rate constant (k_d) for these experiments. In

295 the case of intestinal dissolution profiles generated after two-stage testing, the first-order

296 disintegration option was deactivated since disintegration in the stomach had been already accounted

297 for by the dissolution in the gastric medium. For dissolution experiments of the pure drug, the

298 disintegration time was assumed to be negligible.

299 Estimation of the relevant parameters was performed using the Nelder-Mead algorithm and equal

300 weighting was applied. The various estimated S_{DLM} and k_d values were implemented in the Simcyp®

301 Simulator (V18.1; Certara, Sheffield, UK) to simulate various *in vivo* dissolution scenarios for the

302 formulations under study and to generate *in vitro-in vivo* extrapolation relationships. These are

303 necessary to predict the formulation or pure drug *in vivo* performance using PBPK modelling.

2.8 *In vivo* studies

Seven clinical trials published in the open literature were used in support of the development and verification of the PBPK model for naproxen. Six studies were performed after oral administration of single-dose of naproxen or its sodium salt at different dose levels in the fasted state. Data after intravenous administration were obtained from Runkel et al.(Runkel et al., 1973, 1972a, 1972b)

The results of bioavailability studies for the Naprosyn® formulation were published by Charles and Mogg(Charles and Mogg, 1994) and by Zhou et al.(Zhou et al., 1998) In the study by Charles and Mogg, sixteen Caucasian (12.5% females) healthy subjects with mean (SD) age of 22.1 (4.4) years old received one 500 mg Naprosyn® tablet with 100 mL water at 8:00 a.m. after an overnight fast. All individuals were within 20% of their ideal body weight for height and gender with a mean (SD) weight and height of 67.6 (8.3) kg and 175.7 (9.0) cm, respectively. In the study by Zhou et al., ten Chinese healthy male volunteers (with age and body weight ranging from 19-38 year and 51-74 kg respectively) received two 250 mg Naprosyn® tablets with 200 mL water at 8 a.m. after an overnight fast.

Regarding the Anaprox® formulation, a bioavailability study by Haberer et al.(Haberer et al., 2010) and a bioequivalence (BE) study by Setiawati et al.(Setiawati et al., 2009) have been reported in the literature. Using the same study design (two-treatments protocol), Haberer et al. tested the bioavailability of a tablet of 550 mg Anaprox® as well as of 500 mg of naproxen sodium, with the intention of incorporating this dose in a fixed dose combination tablet with sumatriptan. A tablet of 550 mg Anaprox® (treatment A) and of 500 mg of naproxen sodium (treatment B) were administered after an overnight fast to 8 and 16 healthy non-smoker volunteers, respectively. The proportion of females in the study was 63% and subjects had a mean (SD) age of 44.3 (8.5) years and a mean body weight of 71.44 (12.3) kilograms. In the study by Setiawati et al., twenty-six healthy volunteers (15% females), aged 19 to 46 years and with body mass index (BMI) 18-23, were administered a tablet

328   containing 550 mg naproxen sodium with 200 mL of water in a sitting position at 07:00 a.m. after an

329   overnight fast.

330   To investigate the bioavailability of naproxen free acid, Rao et al. administered 500 mg of pure drug

331   powder filled in hard capsules together with a glass of water to twelve Indian healthy male volunteers,

332   aged between 18 and 22 years, who had fasted overnight.(Rao et al., 1993) In all studies, no

333   concomitant administration of any other drugs was permitted for at least 1 week before the study and

334   food was withheld until 3 hours post-dose.

335   All available demographic data from the aforementioned clinical studies were used to simulate the

336   clinical trials and are summarized in Table 2. Since no pharmacokinetic differences due to race have

337   been identified to date, all individuals were treated the same in terms of ethnicity for modeling

338   purposes.

339

340   *Table 2: Mean (SD) demographic data of in vivo studies used for the development and verification of the PBPK model. (HV= healthy volunteers)*

341

342

2.9 Development of the middle-out PBPK model and selection of *in silico* input parameters

345

346   PBPK modeling and simulations were performed using the Simcyp® Simulator (V18.1; Certara,

347   Sheffield, UK). The naproxen PBPK model was developed by implementing a stepwise sequential

348   modeling strategy, in line with previously published literature and the regulatory guidelines.(European

349   Medicines Agency (EMA), 2018b; Ke et al., 2016; Kuepfer et al., 2016; Shebley et al., 2018; U.S.FDA

350   Center for Drug Evaluation and Research (CDER), 2018b; Zhao et al., 2012) Initially, an intravenous (IV)

351   model was set up and, after optimizing the distribution/elimination parameters, it was adapted to

352   mechanistically describe oral absorption. The compound file was also informed with physicochemical

353   parameters including molecular weight (MW), octanol:water partition coefficient ($logP_{o:w}$), fraction

354   unbound in plasma (f_u) and blood to plasma ratio (B:P) obtained from the literature.(Bergström et al.,

355   2014; Brown et al., 2007; Davies and Anderson, 1997; Lin et al., 1987; Paixão et al., 2012; Pérez et al.,

356   2004; Zhao et al., 2001)

357

358   2.9.1   Intravenous (IV) model

359

360   Since the volume of distribution reported in the literature for naproxen usually lies between 0.05-0.2

361   L/kg (similar to the plasma water volume),(Awni et al., 1995; Franssen et al., 1986; Gøtzsche et al.,

362   1988; Niazi et al., 1996; Upton et al., 1984; Van den Ouweland et al., 1988; Vree et al., 1993) the

363   minimal PBPK (mPBPK) with a single adjusting compartment (SAC) was chosen as the distribution

364   model. The mPBPK is a "lumped" PBPK model in which the SAC represents all tissues excluding liver

365   and portal vein. Use of the SAC requires prior fitting to observed clinical data using the Simcyp®

366   parameter estimation (PE) module. Implementing a "middle-out" strategy, the post-absorptive

367   variables, i.e. the parameter values for volume of distribution at steady-state (V_{ss}), apparent SAC

368   volume (V_{sac}), inter-compartmental (Q_{sac}) and *in vivo* IV clearance (CL_{IV}) were estimated using the

369   PE module after simultaneous fitting of the mPBPK model to the observed intravenous data.(Runkel et

370   al., 1973, 1972a, 1972b) The estimation was weighted by the number of individuals in the reported

371   study and the resulting parameters were then compared with values reported in the literature.

372   2.9.2   p.o. (oral) model

373

374   For mechanistic absorption modeling the advanced dissolution absorption and metabolism (ADAM)

375   model,(Jamei et al., 2009; S. Darwich et al., 2010) in which the gastrointestinal tract (GIT) is divided

376   into 9 anatomically distinct segments starting from stomach through small intestine to the colon, was

377   used. It was assumed that no drug absorption in the stomach occurred. The effective permeability

378   ($P_{eff,man}$) value in humans was obtained from the literature,(Lennernas et al., 1995) whereas for S_0,

379   $logK_{m:w,unionized}$, $logK_{m:w,ionized}$ the estimates from model-based analysis of the *in vitro* solubility

380   data were implemented (see section 2.7). Default settings of the software for luminal blood flow, fluid

381   volume, bile salt content, segmental pH, metabolic activity and small intestinal residence time were

382   used. The mean gastric emptying time (GET) in the fasted state was set to 0.25 h (matching the built-

383   in 'segregated transit time' model value instead of the default value of 0.4 h used in the 'global' transit

384   time model), as suggested by human clinical data and several authors.(Cristofoletti et al., 2016; Hens

385   et al., 2014; Paixão et al., 2018; Psachoulias et al., 2011) All relevant input parameters for the

386   development of the PBPK models and simulations are summarized in Table 3.

387   *Table 3: Input parameters for naproxen PBPK model development and simulations*

388

389   ## 2.10 Verification of PBPK model and Clinical Trial simulations

390

391   The performance of the developed PBPK model was verified by simulation of several clinical studies

392   after oral administration and by comparison with the mean observed pharmacokinetic profiles already

393   available in the literature.(Charles and Mogg, 1994; Haberer et al., 2010; Rao et al., 1993; Setiawati et

394   al., 2009; Zhou et al., 1998) Virtual populations were selected to closely match the enrolled individuals

395   in the respective *in vivo* clinical trials with respect to sample size, ethnicity, gender ratio, and age and

396   weight range. Reported volumes of concomitant liquid intake, dosage form type and sampling

397   schedule were also included in the study design.

398 Using an *in vitro-in vivo* extrapolation (IVIVE) approach, the various DLM scalar estimates, (see sections

399 2.7, 3.5) obtained by model-based analysis of the *in vitro* dissolution data with the diffusion layer

400 model were input to best capture different *in vivo* dissolution scenarios. Further, to investigate the

401 effect of *in vivo* dissolution of multiple formulations and under various conditions on the overall *in vivo*

402 performance, the same DLM scalar estimates from *in vitro* dissolution data for each case were

403 implemented to simulate the aforementioned clinical studies. Every *in vivo* dissolution scenario was

404 evaluated by simulating of 10 trials, each with 10 subjects each (Σ=100). All virtual clinical trials were

405 matched in terms of demographic data (e.g. gender ratio, age & weight range) as closely as possible to

406 the reported studies.

407 ## 2.11 Parameter Sensitivity Analysis (PSA)

408

409 Once confidence in the PBPK model performance was established, parameter sensitivity analysis (PSA)

410 was conducted to identify the absorption rate limiting steps and their impact on *in vivo* performance

411 (e.g., C_{max}, t_{max}, AUC). Variation of one or two parameters at a time over a physiologically realistic range

412 of values was applied for gastric emptying time (GET) and the DLM scalar.

413

414 ## 2.12 Virtual Bioequivalence (VBE) Trials

415

416 The virtual bioequivalence (VBE) trials were designed as fully replicated, two-sequence, two-

417 treatment, two-period, crossover studies. In virtual BE studies between the hypothetical test and

418 reference formulations, PK profiles for a total of 120 healthy adult volunteers (12 subjects in each of

419 10 trials) for each treatment were generated. The existing default coefficients of variation (%CV) - i.e.,

420 between subject (BS) variability of the physiological parameters stored in the Simcyp® simulator

421 database for the North European Caucasian healthy adult volunteers' population were applied for each

422   parameter. As an integral part of within-subject (WS) variability, inter-occasion variability (IOV)

423   significantly contributes to the overall population variability and therefore it should be accounted for

424   by the PBPK models. To model IOV, a CV of 30% was set, according to the literature and unpublished

425   data from C. Reppas.(Fruehauf et al., 2007; Grimm et al., 2018; Lartigue et al., 1994; Petring and Flachs,

426   1990) IOV was added through the VBE module (V1.0) of Simcyp® simulator to the mean GET, pH of

427   fasted stomach, pH and bile salts concentration of fasted duodenum, jejunum I and II segments and

428   mechanistically propagated in the simulations. The IOV was intentionally set to the somewhat

429   exaggerated value of 30% for all the relevant parameters to further challenge the establishment of

430   bioequivalence. In each trial, a pre-specified number of randomly simulated individuals (n=12) were

431   generated for each formulation (reference and test). The relevant PK metrics (C_{max}, t_{max}, AUC) for each

432   subject were calculated. The VBE trials were interpreted as crossover studies and average BE (ABE)

433   was assessed using Phoenix® WinNonlin (v8.1; Certara; Princeton, NJ, USA) for each relevant PK metric.

434   In a best-and worst-case scenario the hypothetical reference and test formulations were assumed to

435   have *in vivo* dissolution in the virtual individuals corresponding to the highest and lowest estimated

436   DLM scalar value, respectively, resulting from the model-based analysis of the *in vitro* dissolution data.

437   ## 2.13 Data Analysis and Model Diagnostics

438

439   The solubility and dissolution data are presented as the arithmetic mean with standard deviations.

440   Model-based analysis of the *in vitro* data in SIVA® Toolkit was performed with either the Nelder Mead

441   or the hybrid algorithm (genetic algorithm coupled to Nelder Mead) with a 5th order Runge-Kutta or

442   Livermore solver. Different weighting schemes were tested and the goodness of fit was assessed by

443   the Akaike (AIC, AICc) and Bayesian (BIC) information criteria as well as the coefficient of determination

444   (R squared). All PK profiles obtained from the literature were digitalized with the WebPlotDigitizer

445   (version 4.1; PLOTCON; Oakland, USA). The estimation of the post-absorptive parameters within the

446   PE module of the Simcyp® Simulator was performed with the Maximum Likelihood estimation method.

447 The prediction accuracy of the simulated plasma profiles was evaluated with the average fold error

448 (AFE) and absolute average fold error (AAFE) (see Equations 4,5).

$$AFE = 10^{\frac{1}{n}\cdot\Sigma \log\left(\frac{pred_t}{obs_t}\right)} \tag{4}$$

449

$$AAFE = 10^{\frac{1}{n}\cdot\Sigma\left|\log\left(\frac{pred_t}{obs_t}\right)\right|} \tag{5}$$

450

451

452 where n is the number of time points at which the concentration was determined and $pred_t$, obs_t are

453 the predicted and observed concentrations at a given time point t respectively. AFE deviation from

454 unity is an indication of over- ($AFE > 1$) or under-prediction ($AFE < 1$) of the observed data,

455 whereas $AAFE$ is a measure of the absolute error from the true value (or bias of the simulated profile).

456 An $AAFE \leq 2$ is considered to be a successful prediction.(Obach et al., 1997; Poulin and Theil, 2009)

457 Statistical analysis (including 95% CI) and VBE trials were performed with Simcyp® (V18.1; Certara,

458 Sheffield, UK) and Phoenix® WinNonlin (v8.1; Certara; Princeton, NJ, USA). Data post-processing and

459 plotting were performed with MATLAB® 2018a (Mathworks Inc.; Natick, MA, USA) and R® (version

460 3.5.1).

461

3 Results

3.1 *In vitro* solubility

3.1.1 Aqueous Buffers

Table 4 summarizes the equilibrium solubility values in various aqueous media of different pH. In the case of the free acid, the final pH_{bulk} differed significantly from the initial pH values due to the self-buffering effect. This behavior was not observed for the sodium salt, where the pH difference was equal or less to 0.1 pH unit. The higher solubility of the sodium salt compared to the free acid, especially in the intestinal pH media, is attributed to the difference in the final pH measured, keeping in mind that in this pH range the solubility increases exponentially with pH increase. Since naproxen is a weakly acidic compound, its pH-solubility profile is described by two regions: a) $pH < pH_{max}$, where the excess solid phase in equilibrium with the saturated solution consists of the unionized form and b) $pH > pH_{max}$, where the equilibrium species are exclusively in the ionized form.(Avdeef, 2007) Hence, unless self-association of solute molecules occurs, identical pH-solubility profiles at equilibrium are expected regardless of the starting material (free acid or salt), as shown in Figure 1. The experimental values were plotted as a pH-solubility profile and compared to values reported in the literature, showing excellent agreement (Figure 1).(Avdeef, 2007; Avdeef and Berger, 2000; Chowhan, 1978)

Table 4: Mean (± SD) equilibrium solubility in aqueous media at 37°C for 24h (Uniprep® method).

486

487 *Figure 1: Naproxen (squares) and naproxen sodium (triangles) experimental mean equilibrium solubility values (24 h at 37°C)*

488 *plotted against respective literature values (24 h at 25°C) in a pH-solubility profile. The in vitro solubility experiments were*

489 *performed with the Uniprep® method described in section 2.2. The experimental results are in agreement with the literature*

490 *values (24 h at 25°C). The literature values were obtained from Avdeef et al. (Ref. 75); Chowhan et al. (Ref. 77)*

491

492 ### 3.1.2   Biorelevant media

493

494 The solubility was additionally investigated in selected Level II fasted and fed state biorelevant media

495 (see Table 5).(Markopoulos et al., 2015) Similar to the solubility of the free acid in phosphate buffers,

496 a considerable decrease in the final pH_{bulk} was observed in fasted state biorelevant media. In fact, the

497 reduction is even more pronounced in the fasted state biorelevant media due to their lower buffer

498 capacity (5.6 mmol/L/ΔpH in FaSSIF V3 *versus* 18.5 mmol/L/ΔpH in European Pharmacopoeia

499 phosphate buffers).(Fuchs et al., 2015) Comparison of solubilities in compendial with those in

500 biorelevant media shows that micelle-mediated solubilization has a substantial impact on the overall

501 solubility of naproxen. Particularly in FaSSIF V1 Level II, the solubility of both free acid and sodium salt

502 was increased by 25.8% and 51.8%, respectively, when compared to phosphate buffer (pH=6.5).

503 Likewise, in media simulating the fed state, such as FeSSIF V1 Level II, a 2.4-fold increase in the

504 solubility of the free acid and a 2.1-fold increase for the salt form were observed, in comparison to the

505 respective medium without surfactants.

506

507 *Table 5: Mean (± SD) equilibrium solubility in fasted and fed state biorelevant media at 37°C for 24h (Uniprep® method).*

508

3.2 Modeling of *in vitro* solubility

Table 6 summarizes the parameter estimates (95% CI) obtained by model-based analysis of the *in vitro* solubility data in compendial and biorelevant media, as described in section 2.6. The pK_a was determined to be 4.43, which agrees with values reported in the literature (4.15-4.5). (Avdeef, 2007; Chowhan, 1978; Davies and Anderson, 1997; McNamara and Amidon, 1986; Sheng et al., 2009) By estimating the micelle-water partition coefficients for both neutral and ionized species using the biorelevant solubilities, we were able to quantify the effect of physiologically relevant surfactants on the overall solubility of naproxen. These values were utilized within the Simcyp® Simulator to simulate the luminal conditions and the *in vivo* dissolution behavior, accounting at the same time for any inter-subject variability regarding bile salt-mediated solubilization in the virtual population. Therefore, implementation of $logK_{m:w}$ neutral and ion in the PBPK model allowed for mechanistic prediction of the *in vivo* luminal dissolution, which would not be possible if only mean solubility values had been used.

Table 6: Parameter estimates (95% CI) resulting from the model-based analysis of in vitro solubility data in aqueous as well as biorelevant media. The pka was estimated from the aqueous solubility values, whereas for the micelle-water partition coefficients ($logK_{m:w}$ neutral, ion) estimation, biorelevant solubilities were used. The accuracy of the predictions was evaluated with the R squared.

3.3 *In vitro* dissolution tests

3.3.1 Active Pharmaceutical Ingredient (API) powder

532   Mean percentage dissolved (± SD) over time in compendial and fasted state biorelevant media for the

533   pure API of naproxen and its sodium salt are presented in Figure 2 and Figure 3, respectively. All

534   dissolution experiments were performed as described in section 2.3.

535   For the free acid, dissolution in FaSSIF V3 Level II and in Ph. Eur. phosphate buffer pH=6.8 was very

536   rapid (>85% within 5 minutes in FaSSIF V3) and rapid (>85% within 30 minutes in phosphate buffer).

537   On the other hand, the dissolution in FaSSIF V3 Level I (i.e. without bile components) was much slower

538   with 85% dissolved reached only after 60 minutes. The observed differences in *in vitro* dissolution

539   behavior is attributed to differences in buffer capacity (FaSSIF V3 Level I and II vs. phosphate buffer)

540   and solubilization capacity (FaSSIF V3 Level II vs. Level I) of the tested media, whereas the difference

541   of 0.1 pH units between the initial pH of Ph. Eur. phosphate buffer pH=6.8 and FaSSIF V3 is assumed

542   to have a negligible effect.

543   Especially since dissolution was under non-sink conditions in this series of experiments, the dissolution

544   rate in FaSSIF V3 Level I was significantly slower, due to its low buffer capacity (5.6 mmol/L/ΔpH), than

545   in the compendial phosphate buffer (13.5 vs. 50 mM phosphate buffer). At higher total phosphate

546   buffer concentration, i.e. in the compendial medium, the bulk (pH_{bulk}) rather than the surface pH (pH_0)

547   drives solubility and dissolution. By contrast, in the low buffer capacity FaSSIF V3 Level I medium the

548   surface pH seems to control the dissolution rate and as a result the final pH is significantly altered (5.95

549   in FaSSIF V3 Level I vs. 6.62 in Ph. Eur. phosphate buffer). The effect of buffer capacity on the overall

550   dissolution behavior becomes much less prominent when bile salts are added to the medium, as shown

551   in Figure 2. Furthermore, it is evident that the addition of the bile salt components in FaSSIF V3 Level

552   II markedly enhances the dissolution rate. Although the main effect is likely through solubilization,

553   improvements in wetting may have also contributed to the higher dissolution rate in the Level II

554   medium.

555   For the sodium salt, these trends were not observed and dissolution was almost instantaneous (85%

556   dissolved by the first sampling time at 2.5 min) in all tested media. This is attributed to the higher

557   solubility as well as higher surface pH generated by the sodium salt of naproxen.

558

Figure 2: In vitro dissolution (mean ± SD) of 500 mg naproxen free acid API powder in Ph. Eur. phosphate buffer (pH=6.8), Level I and II FaSSIF V3. USP paddle apparatus at 75 rpm and 500 mL of dissolution medium at 37°C were used in all experiments. The experiments were performed in triplicate. Horizontal dashed red line represents 85% dissolved. Most standard deviation bars lie within the symbols.

559

560   *Figure 3: In vitro dissolution (mean ± SD) of 550 mg naproxen sodium API powder in Ph. Eur. phosphate buffer (pH=6.8), FaSSIF*

561   *V3 Levels I and II. USP paddle apparatus at 75 rpm and 500 mL of dissolution medium at 37°C were used in all experiments.*

562   *The experiments were performed in triplicate. Horizontal dashed red line represents 85% dissolved. Most standard deviation*

563   *bars lie within the symbols.*

564

565   3.3.2   Formulations

566

567   The dissolution profiles in FaSSIF V3 Levels I and II along with the results for the "intestinal" part of the

568   two-stage testing are presented for Naprosyn® and Anaprox® in Figure 4 and Figure 5, respectively. In

569   all cases, and for both formulations, dissolution was very rapid under conditions simulating the upper

570   small intestine, with 85% dissolved in less than 15 min. Interestingly, a mismatch between the

571   dissolution results of the APIs and dosage forms was observed. For instance, dissolution of the free

572   acid form of the API was much faster from the dosage form (Naprosyn®) than from the pure API in

573   FaSSIF V3 Level I. However, the dissolution of naproxen free acid from Naprosyn® in FaSSIF V3 Level II

574   was slightly slower than from the pure API. Furthermore, although dissolution of sodium salt API was

575   virtually instantaneous in all media (85% dissolved within 2.5 min), 85% dissolution was reached only

576   after 15 minutes during release from Anaprox®.

577 These findings suggested that the dissolution of the tablets under intestinal conditions was delayed

578 due to slow disintegration, especially in the case of the sodium salt formulation. In order to account

579 for disintegration in the stomach prior to exposure to the intestinal media, two-stage dissolution tests

580 were subsequently performed, as described in section 2.4. Since the amount dissolved under gastric

581 conditions was less than 2% in all cases (see Figure 6), only the "intestinal" profiles of the 2-stage tests

582 are plotted and directly compared with the conventional dissolution profiles (Figure 4 and Figure 5).

583 Pre-treatment in gastric media accelerated the dissolution rate (85% dissolved reached 5 min earlier)

584 of the API from both the Naprosyn® formulation of the free acid (Figure 4) and the Anaprox®

585 formulation of the sodium salt form (Figure 5). Although in all cases dissolution would be considered

586 very rapid, the disintegration effect was more prominent for Anaprox®, as shown also in Figure 6. A

587 model-based analysis of the anticipated in vitro dissolution differences is presented in section 3.4.

588

589 *Figure 4: In vitro dissolution (mean ± SD) of Naprosyn® 500 mg in FaSSIF V3 Levels I and II (solid lines, filled squares and circles*

590 *respectively). The intestinal profiles in FaSSIF V3 Levels I and II (after the pre-treatment with FaSSGF Levels I and III respectively)*

591 *during two-stage test are also depicted (dotted lines, empty squares and circles, respectively). USP paddle apparatus at 75*

592 *rpm and 500 mL of dissolution medium at 37°C were used in all experiments. The experiments were performed in triplicate.*

593 *Horizontal dashed red line represents the 85% dissolved. Most standard deviation bars lie within the symbols*

594

595 *Figure 5: In vitro dissolution (mean ± SD) of Anaprox® 550 mg in FaSSIF V3 Levels I and II (solid lines, filled squares and circles*

596 *respectively). The intestinal profiles in FaSSIF V3 Levels I and II (after the pre-treatment with FaSSGF Levels I and III respectively)*

597 *during two-stage test are also depicted (dotted lines, empty squares and circles, respectively). USP paddle apparatus at 75*

598 *rpm and 500 mL of dissolution medium at 37°C were used in all experiments. The experiments were performed in triplicate.*

599 *Horizontal dashed red line represents the 85% dissolved. Most standard deviation bars lie within the symbols*

600

601

602

603

604

Figure 6: In vitro dissolution (mean ± SD) of Naprosyn® 500 mg (solid lines) and Anaprox® 550 mg (dashed lines) in FaSSGF Levels I and III (filled circles and squares, respectively). USP paddle apparatus at 75 rpm and 250 mL of dissolution medium at 37°C were used in all experiments. The experiments were performed in triplicate. Horizontal dashed red line represents the 85% dissolved. Most standard deviation bars lie within the symbols.

605

3.4   Modeling of *in vitro* dissolution

607

608   Table 7 and Table 8 summarize the estimated DLM scalar values (95% CI) obtained by model-based

609   analysis of the intestinal *in vitro* dissolution profiles using the SIVA Toolkit®. Each naproxen form (i.e.

610   pure API and formulations of each of the free acid and sodium salt) was evaluated separately. The

611   goodness of fit was visually inspected with residuals plots and assessed with the coefficient of

612   determination (R^2). As shown in Table 8, the first-order disintegration model without time-lag was

613   applied only to those experiments where the formulations were not pre-exposed to gastric medium.

614   Matching between two-stage and single dissolution, combined with the disintegration model, DLM

615   estimates were obtained. These results indicate that the effect of disintegration can be properly

616   accounted for using the methodology applied.

617   The slowest and fastest dissolution rate of the acid form of the API observed in FaSSIF V3 Levels I and

618   II, respectively, resulted in the lowest (0.0022) and highest (0.0810) estimated DLM values. Due to the

619   virtually instantaneous dissolution of the sodium salt API in all media, the default DLM value of 1,

620   without estimation, was utilized for the salt form (Table 7). The predicted dissolution profiles were in

621   excellent agreement with the experimental profiles ($R^2 > 0.96$).

622

623 *Table 7 : Estimated DLM scalar values (95% CI) obtained from model-based analysis of in vitro dissolution in various media of*

624 *naproxen free acid and sodium salt pure API powder. The goodness of fit between predicted and observed dissolution profiles*

625 *was evaluated with the R squared (R^2).*

626

627 *Table 8: Estimated DLM scalar and first-order disintegration rate constant (k_d) values (95% CI) obtained from model-based*

628 *analysis of in vitro dissolution in various media of naproxen free acid (Naprosyn®) and sodium salt (Anaprox®) formulation. In*

629 *case of dissolution without pre-treatment in a gastric medium, a first-order disintegration model was included. The goodness*

630 *of fit between predicted and observed dissolution profiles was evaluated with the R squared (R^2).*

631

632 3.5 PBPK model verification & clinical trial simulations

633

634 The PBPK model of naproxen was developed and verified as described in sections 2.9 and 2.10,

635 respectively. Post-absorptive parameters (CL, V_{ss}, V_{sac}, Q_{sac}) were estimated from intravenous data,

636 whereas for dissolution-absorption the Diffusion layer model-ADAM was used. Different *in vivo*

637 dissolution scenarios were simulated according to the DLM scalar values obtained by model-based

638 analysis of *in vitro* biorelevant dissolution profiles of the tested naproxen forms. The simulated profiles

639 were compared against observed data from human *in vivo* PK studies (see section 2.8). The generated

640 virtual population closely matched the individuals enrolled in the respective *in vivo* studies in terms of

641 ethnicity, gender ratio, and age and weight range. Volumes of concomitant liquid intake, dosage form

642 type and sampling schedule were also taken into account for the virtual study design wherever

643 available (see details in section 2.10).

644 Table 9 summarizes all the simulations (10 trials by 10 individuals) performed for each *in vivo*

645 dissolution scenario and the resulting mean *in silico* population pharmacokinetic (popPBPK)

646 parameters for the virtual healthy adult population. Regardless of the anticipated differences in *in vivo*

647 dissolution, as reflected by the various estimated DLM values, these results suggest that mean AUC

648 remains almost constant, while more pronounced variations in C_{max} and especially in t_{max} are observed.

649   Direct comparisons of the mean *in silico* and *in vivo* pharmacokinetic parameters show very good

650   agreement between simulated and observed data (Table 9 and Table 10). In all cases, the average (AFE)

651   and absolute average fold error (AAFE) lay between 0.90-1.16 and 1.07-1.04, reflecting successful PBPK

652   model performance and excellent predictions of the observed plasma profiles.

653   Figure 7 illustrates the mean simulated naproxen plasma-concentration time profiles and the 5th and

654   95th percentiles of the virtual population for the two extreme DLM estimated values; i.e.,

655   DLM_{min}=0.0022 and DLM_{max} = 1. Note that these DLM values were extracted from the dissolution of

656   the free acid and salt pure API forms, not the formulations, and were intentionally chosen as such in

657   order to evaluate *in vivo* performance differences (if any) that could be detected under these extreme

658   scenarios. As can be observed, the C_{max} of the simulated plasma profile corresponding to

659   administration of the very slowly dissolving hypothetical formulation was only slightly lower than the

660   one resulting from the very fast dissolving hypothetical formulation. On the other hand, tmax was

661   significantly prolonged. Interestingly, regardless of whether the worst or best case scenario was

662   applied, the dissolution profiles predicted the observed range of PK profiles reasonably well (see also

663   AFE and AAFE values).

664   In order to further explore the impact of key parameters on the simulated plasma profiles, one-at-a-

665   time parameter sensitivity analysis (PSA) on the DLM scalar and GET in the fasted state was performed.

666   GET and DLM were allowed to range from 0.1 to 2 hours and 0.001 to 0.1, respectively, while all other

667   parameters in the model were kept constant. Figure 8 and Figure 9 show the mean simulated plasma

668   profiles of a representative individual of the virtual population for various DLM and GET values,

669   respectively. Figure 8 shows that over a 100-fold range of DLM values only slight or almost no

670   differences in C_{max} (69.7-74.0 mg/L) or AUC (1175-1177 mg/L $\cdot$ h) are observed. T_{max} (1.40-2.65 h) seems

671   to be more sensitive to *in vivo* dissolution changes (as reflected in the S_{DLM} values) than the other PK

672   parameters. Figure 9 clearly demonstrates that variation in GET markedly affects C_{max} (52.2-75.5 mg/L)

673   and t_{max} (1.09-4.00 h), whereas AUC (1172-1180 mg/L $\cdot$ h) is not impacted.

674   As one would anticipate, PSA on dissolution rate in the stomach revealed no changes in the simulated

675   C_{max}, t_{max} and AUC (data not shown), since poorly soluble weakly acidic compounds like naproxen barely

676   dissolve in the fasted state gastric environment (see also Figure 6).

677

678   *Table 9: Mean in silico population pharmacokinetic (popPBPK) parameters of naproxen simulated plasma-concentration-*

679   *time profiles under all tested in vivo dissolution inputs (DLM scalar values) as obtained from model-based analysis of the in*

680   *vitro data (see formulation and dissolution medium).*

681

682   *Table 10: Mean (SD) pharmacokinetic parameters of naproxen in vivo studies ([a] Median value).*

683

Figure 7: Population mean simulated naproxen plasma concentration-time profiles and the 5th and 95th percentiles for the two extremes of the estimated S_{DLM} values: (a) S_{DLM}=1 (green and grey solid lines, respectively) and (b) DLM=0.0022 (blue and light grey dashed lines, respectively). In a worst/ best case virtual bioequivalence scenario of simulated healthy adult populations (a) was treated as the reference, whereas (b) as the test formulation. Observed clinical data from Charles & Mogg (circles), Zhout et al. (squares), Haberer et al. (a) (diamonds), Setiawati et al. (triangles), Rao et al. (crosses) and Haberer et al. (b) (asterisks) are overlaid for verification of the PBPK model performance and comparisons. Simulations run for 72 h, but to enable better comparison only the first 24 hours are plotted.

684

685

Figure 8: Sensitivity analysis of naproxen simulated plasma concentration-time profiles of population representative individual on DLM scalar values ranging from 0.001 (blue solid line) to 0.1 (dashed line). The values of all other parameters were kept constant (GET=0.25 h). Observed clinical data from Charles & Mogg (circles), Zhout et al. (squares), Haberer et al. (a) (diamonds), Setiawati et al. (triangles), Rao et al. (crosses) and Haberer et al. (b) (asterisks) are overlaid for comparisons. Simulations run for 72 h, but to enable better comparison only the first 24 hours are plotted.

686

687

Figure 9: Sensitivity analysis of naproxen simulated plasma concentration-time profiles of population representative individual on GET values in fasted state ranging from 0.1 (blue solid line) to 2 hours (dash double dotted line). The values of all other parameters were kept constant (DLM= 1). Observed clinical data from Charles & Mogg (circles), Zhout et al. (squares), Haberer et al. (a) (diamonds), Setiawati et al. (triangles), Rao et al. (crosses) and Haberer et al. (b) (asterisks) are overlaid for comparisons. Simulations run for 72 h, but to enable better comparison only the first 24 hours are plotted.

688

3.6 Virtual Bioequivalence

690

Multiple non-replicated, two-sequence, two-treatment, two-period, cross-over virtual bioequivalence trials (n=10) with 12 individuals per trial were conducted. In a worst/ best case scenario, two hypothetical naproxen formulations with extremely different *in vivo* dissolution rates were tested with the aim of designing a clinically relevant safe space. The reference (R) was assumed to have a DLM scalar value of 1, corresponding to the instantaneous dissolution of naproxen sodium API powder, while the test (T) formulation was assigned the value of 0.0022, corresponding to the very slow dissolution of naproxen free acid API powder in FaSSIF V3 Level I (Table 11).

Figure 10 presents the results of virtual bioequivalence trials for C_{max}, AUC calculated up to the last simulated time point (AUC_{tlast}) and extrapolated to infinity (AUC_{inf}). Bioequivalence with regard to t_{max} was also investigated. In all trials, C_{max}, AUC_{tlast}, AUC_{inf} met the average bioequivalence criteria (80-125%) with confidence intervals (CI) narrowly distributed around unity, especially for AUC. However, in terms of t_{max} bioequivalence failed in all 10 trials and most CI were far beyond the bioequivalence limits. These findings suggest that naproxen formulations which reach 85% dissolved in media simulating the healthy human upper small intestine within 90 minutes or less are expected to be bioequivalent. These borders correspond to the dissolution "safe space" and can be used to set clinically relevant dissolution specifications to minimize the risk of bioequivalence failure.

707   *Table 11: Mean in silico population pharmacokinetic (popPBPK) parameters of naproxen virtual clinical trials for the*

708   *hypothetical reference and test formulations prior to bioequivalence assessment.*

709

710

Figure 10: Average virtual bioequivalence results (% Geometric mean T/R ratio) of 10 trials with 12 simulated individuals in each trial. Intra-subject variability of 30% was arbitrarily chosen and added through Simcyp ® (V18.1; Certara, Sheffield, UK) VBE module (V1.0) to the mean GET, pH of fasted stomach, pH and bile salts concentration of fasted duodenum, jejunum I and II. The 80-125% bioequivalence limits (red dashed lines) and the area of acceptance (light green shaded area) are shown for each tested PK parameter: (A) C_{max}, (B) AUC_{tlast} (AUC calculated up to the last simulated time point), (C) AUC_{inf} (AUC extrapolated to infinity) and (D) t_{max}. Error bars represent the 90% confidence intervals, which in subplots (B) and (C) lie within the symbols.

Figure 11: Dissolution safe space for anticipated bioequivalence to naproxen products. The light green shaded area delimits the safe space area in which bioequivalence (with respect to C_{max} and AUC) was established between the very slow (red solid line & squares) and the fast (blue solid line & circles) dissolution profiles. Additional typical dissolution profiles are co-plotted (n=3). The horizontal red dashed line represents 85% dissolved.

713

4 Discussion

715

716 The present study proposes a workflow and highlights the key role of mechanistic absorption and

717 population-based PBPK modeling to establish virtual bioequivalence and set clinically relevant

718 dissolution specifications by combining *in vitro*, *in vivo* and *in silico* methods.

719 In the naproxen case example, starting from *in vitro* solubility and dissolution data, an approach of

720 stepwise sequential estimation/confirmation of biopharmaceutical parameters was followed,(Pathak

721 et al., 2019) before applying them to the PBPK model. *In vitro* dissolution profiles in conventional and

722 biorelevant media were translated to different *in vivo* dissolution scenarios by implementing an *in*

723 *vitro-in vivo*-extrapolation (IVIVE) strategy. The healthy adult PBPK model for naproxen was developed

724 by optimizing post-absorptive parameters from intravenous in vivo data which was then coupled with

725 the ADAM model for mechanistic oral absorption modelling. The verification of the PBPK model was

726 based on its ability to predict the observed plasma PK profiles after oral administration of naproxen in

727 several *in vivo* studies and its performance under multiple *in vivo* dissolution scenarios was assessed.

728 Simulations of the clinical studies in conjunction with sensitivity analysis on the DLM scalar and gastric

729 emptying time revealed that C_{max} and AUC are rather insensitive to dissolution changes, but that C_{max}

730 is considerably affected by variations in gastric emptying time. However, changes in either the S_{DLM} or

731 gastric emptying markedly altered t_{max}. These results indicate that the absorption and thus the *in vivo*

732 performance of naproxen formulations seem to be governed by gastric emptying, but is not

733 dissolution-limited. This is supported by the (refined) developability classification system (DCS/

734 rDCS),(Butler and Dressman, 2010; Rosenberger et al., 2019) according to which naproxen would more

735 appropriately be classified as rDCS/ DCS I, and is in excellent agreement with the study of Charles and

736 Mogg(Charles and Mogg, 1994), which concluded that two naproxen products (tablet and caplet) with

737   very dissimilar *in vitro* dissolution behavior were bioequivalent. Furthermore, a DLM scalar range from

738   0.0022 to 1 translated to an increase in C_{max} only by 1.06 and 1.75 times earlier t_{max}, assuming the

739   default in Simcyp particle radius of 10 µm. The AUC remained unchanged. In this case, the insensitivity

740   of PK metrics to the dissolution rate was attributed both to the absence of saturable first pass

741   extraction and the relatively long half-life ($t_{1/2} \approx 20$ h) of the drug.

742   Once enough confidence with the performance of the PBPK model was achieved, several VBE trials

743   simulating a worst/best case scenario were performed. A safe space and a clinically relevant

744   dissolution specification for naproxen products was proposed based on the outcome of these virtual

745   trials. It was demonstrated that 85% dissolved reached within 90 minutes lies comfortably within a

746   region of dissolution performance where bioequivalence is anticipated and is not anywhere near the

747   edge of failure for either C_{max} or AUC. On the other hand, bioequivalence in t_{max} failed in all cases. In

748   this study, *in vitro* dissolution of unformulated free acid and sodium salt forms of naproxen were used

749   to simulate the worst/best case BE scenario. Although this constitutes an extreme limitation, it was

750   done intentionally to challenge the VBE result, since if the VBE were to be based solely on the

751   dissolution of the formulations, the safe space would be biased towards an already (partly) optimized

752   formulation range.

753   Virtual bioequivalence studies have been already published in the recent past(Babiskin and Zhang,

754   2015; Doki et al., 2017; Pathak et al., 1997; Pepin et al., 2016; Wedagedera et al., 2017; Zhang et al.,

755   2017) However, in most of those studies the intra-subject (IIV) and inter-occasion (IOV) variability is

756   either ignored or added directly to the PK metrics (i.e. C_{max} and AUC) as random error terms. By

757   contrast, in the current study the intra-subject variability was added via the Simcyp® v18.1 VBE module

758   1.0 in several key absorption parameters, such as gastric emptying time, pH of fasted stomach, pH and

759   bile salts concentration of fasted duodenum, jejunum I and II, and mechanistically propagated in

760   simulations. In the context of challenging the establishment of bioequivalence, IOV was set to a

761   somewhat exaggerated value of 30% for all parameters.

762

763

5   Conclusion

765

Mechanism-based absorption PBPK modeling can be considered as a promising and powerful bioequivalence risk assessment tool. This work highlights the importance of linking translational absorption modeling with population PBPK to examine VBE and set clinically relevant specifications. For naproxen, it was demonstrated that bioequivalence failure due to dissolution is unlikely for naproxen products because of the wide safe space. The example of naproxen illustrates that the impact of formulation on the *in vivo* performance is not always correlated with the *in vitro* dissolution behavior.

To the best of our knowledge, this is the first work which not only mechanistically incorporates inter-occasion variability in VBE assessment, but also propagates IOV in the simulations. Implementation of hierarchical levels of variability (BS, WS, IOV) in VBE trials is of critical importance in order to accurately describe the population variability and avoid biased, overoptimistic bioequivalence results due to underestimation of the overall variability. Even though mixed effect modelling is rare in this context, this study highlights the importance of mechanistically assigning between-subject and inter-occasion variability values which are physiologically plausible and meaningful. Using %CV values obtained from single observation in each individual within a specific population is not representative of the population BS or IOV since it comes solely from a single sample. In this case, the applied coefficient of variation is often conveniently misinterpreted as mixture of BS and IO variability. Likewise, implementation of arbitrary CV% values is inappropriate.

Moving a step further towards linking the lab to the patient, mechanistic extrapolation of in vitro data (e.g. dissolution) to the in vivo situation, as explicitly demonstrated for naproxen, is critical for the

786 validity and interpretation of VBE results. In the context of bioequivalence trial simulation, which is of

787 great interest for both regulatory agencies and the pharmaceutical industry, a mechanistic IVIVE

788 approach will be essential to enable extrapolation to specific or disease populations, given that

789 differences in factors like GI physiology need to be taken into account. The acquisition of further clinical

790 data (e.g., intraluminal and plasma concentrations) as well as advancement of the current

791 biopharmaceutic tools are expected to significantly increase the reliability of virtual bioequivalence

792 results in a variety of diseases, dosing conditions such as PPI co-administration and specific populations

793 such as pediatric patients.

794 Consideration of drug-related pharmacokinetic characteristics (e.g., half-life, first pass effect, protein

795 binding) along with PBPK modeling will assist not only to select the most appropriate dosage form and

796 to set formulation targets, but more importantly to understand to what extent the formulation can be

797 expected to steer the *in vivo* performance of the drug product. Further validation of the proposed

798 approach with a range of drugs and formulations is needed to increase confidence and spread

799 awareness of the power of mechanistic absorption modeling and PBPK in formulation design and

800 regulation.

801 Bridging the gap between *in vitro*, *in vivo* and *in silico* by applying mechanistic absorption coupled with

802 population PBPK modeling can guide model-informed formulation selection, allow for robust clinical

803 outcome predictions, inform regulatory decision-making, permit regulatory flexibility (e.g. granting

804 biowaivers for some BCS class II weak acids like naproxen) and potentially reduce the cost/time of

805 product development by replacing unnecessary clinical trials.

806 Future work could investigate the impact of bioinequivalence in t_{max} on the onset of action and

807 therefore the therapeutic equivalence of naproxen products. As has already been

808 highlighted,(Cristofoletti et al., 2018; Loisios-Konstantinidis et al., 2019) a scenario is foreseen in which

809 by combining verified PBPK with pharmacodynamic (PD) models tailored to the target population(s),

810 release testing in the laboratory will be linked to the therapeutic outcome.

6 Acknowledgments

7 References

814

815

816   Avdeef, A., 2007. Solubility of sparingly-soluble ionizable drugs. Adv. Drug Deliv. Rev. 59, 568–590.

817   Avdeef, A., Berger, C.M., 2000. pH-Metric Solubility. 2: Correlation Between the Acid-Base Titration

818   and formulations for use in early animal bioavailability and toxicity studies. Later in

819   development, solubility takes on a broader. Pharm. Res. 17.

820   Awni, W.M., Braeckman, R.A., Cavanaugh, J.H., Locke, C.S., Linnen, P.J., Granneman, G.R., Dubé, L.M.,

821   1995. The Pharmacokinetic and Pharmacodynamic Interactions between the 5-Lipoxygenase

822   Inhibitor Zileuton and the Cyclo-Oxygenase Inhibitor Naproxen in Human Volunteers. Clin.

823   Pharmacokinet. 29, 112–124.

824   Babiskin, A.H., Zhang, X., 2015. Application of Physiologically Based Absorption Modeling for

825   Amphetamine Salts Drug Products in Generic Drug Evaluation. J. Pharm. Sci. 104, 3170–3182.

826   Bergström, C.A.S., Andersson, S.B.E., Fagerberg, J.H., Ragnarsson, G., Lindahl, A., 2014. Is the full

827   potential of the biopharmaceutics classification system reached? Eur. J. Pharm. Sci. 57, 224–

828   231.

829   Brown, H.S., Griffin, M., Houston, J.B., Li, A.P., 2007. Evaluation of cryopreserved human hepatocytes

830   as an alternative in vitro system to microsomes for the prediction of metabolic clearance. Drug

831   Metab. Dispos. 35, 293–301.

832   Butler, J.M., Dressman, J.B., 2010. The Developability Classification System: Application of

833   Biopharmaceutics Concepts to Formulation Development. J. Pharm. Sci. 99, 4940–4954.

834   Charles, B.G., Mogg, G.A.G., 1994. Comparative in vitro and in vivo bioavailability of naproxen from

835   tablet and caplet formulations. Biopharm. Drug Dispos. 15, 121–128.

836   Chowhan, Z.T., 1978. pH–Solubility Profiles of Organic Carboxylic Acids and Their Salts. J. Pharm. Sci.

837   67, 1257–1260.

838   Cristofoletti, R., Chiann, C., Dressman, J.B., Storpirtis, S., 2013. A comparative analysis of

839   biopharmaceutics classification system and biopharmaceutics drug disposition classification

840   system: A cross-sectional survey with 500 bioequivalence studies. J. Pharm. Sci. 102, 3136–

841   3144.

842   Cristofoletti, R., Dressman, J.B., 2016. Bridging the Gap Between In Vitro Dissolution and the Time

843   Course of Ibuprofen-Mediating Pain Relief. J. Pharm. Sci. 105, 3658–3667.

844   Cristofoletti, R., Patel, N., Dressman, J.B., 2016. Differences in Food Effects for 2 Weak Bases With

845   Similar BCS Drug-Related Properties: What Is Happening in the Intestinal Lumen? J. Pharm. Sci.

846   105, 2712–2722.

847   Cristofoletti, R., Rowland, M., Lesko, L.J., Blume, H., Rostami-Hodjegan, A., Dressman, J.B., 2018. Past,

848   Present, and Future of Bioequivalence: Improving Assessment and Extrapolation of Therapeutic

849   Equivalence for Oral Drug Products. J. Pharm. Sci. 107, 2519–2530.

850   Davies, N.M., Anderson, K.E., 1997. Clinical pharmacokinetics of naproxen. Clin. Pharmacokinet. 32,

851   268–293.

852   Dickinson, P.A., Lee, W.W., Stott, P.W., Townsend, A.I., Smart, J.P., Ghahramani, P., Hammett, T.,

853   Billett, L., Behn, S., Gibb, R.C., Abrahamsson, B., 2008. Clinical Relevance of Dissolution Testing

854   in Quality by Design. AAPS J. 10, 380–390.

855   Doki, K., Darwich, A.S., Patel, N., Rostami-Hodjegan, A., 2017. Virtual bioequivalence for achlorhydric

856   subjects: The use of PBPK modelling to assess the formulation-dependent effect of

857   achlorhydria. Eur. J. Pharm. Sci. 109, 111–120.

858   European Medicines Agency (EMA), 2018a. Committee for Medicinal Products for Human Use

859   (CHMP) Guideline on the reporting of physiologically based pharmacokinetic (PBPK) modelling

860   and simulation.

861   European Medicines Agency (EMA), 2018b. Committee for Medicinal Products for Human Use

862   (CHMP) Guideline on the reporting of physiologically based pharmacokinetic (PBPK) modelling

863   and simulation.

864   Franssen, M.J., Tan, Y., van de Putte, L.B., van Ginneken, C.A., Gribnau, F.W., 1986. Pharmacokinetics

865   of naproxen at two dosage regimens in healthy volunteers. Int. J. Clin. Pharmacol. Ther. Toxicol.

866   24, 139–42.

867   fruehauf, h., goetze, o., steingoetter, a., kwiatek, m., boesiger, p., thumshirn, m., schwizer, w.,

868   fried, m., 2007. Intersubject and intrasubject variability of gastric volumes in response to

869   isocaloric liquid meals in functional dyspepsia and health. Neurogastroenterol. Motil. 19, 553–

870   561.

871   Fuchs, A., Leigh, M., Kloefer, B., Dressman, J.B., 2015. Advances in the design of fasted state

872   simulating intestinal fluids: FaSSIF-V3. Eur. J. Pharm. Biopharm. 94, 229–240.

873   Gøtzsche, P.C., Andreasen, F., Egsmose, C., Lund, B., 1988. Steady state pharmacokinetics of

874   naproxen in elderly rheumatics compared with young volunteers. Scand. J. Rheumatol. 17, 11–

875   6.

876   Grimm, M., Koziolek, M., Kühn, J.P., Weitschies, W., 2018. Interindividual and intraindividual

877   variability of fasted state gastric fluid volume and gastric emptying of water. Eur. J. Pharm.

878   Biopharm. 127, 309–317.

879   Haberer, L.J., Walls, C.M., Lener, S.E., Taylor, D.R., McDonald, S.A., 2010. Distinct pharmacokinetic

880   profile and safety of a fixed-dose tablet of sumatriptan and naproxen sodium for the acute

881   treatment of migraine. Headache 50, 357–373.

882   Heimbach, T., Laisney, M., Samant, T., Elmeliegy, M., Wu, F., Hanna, I., Lin, W., Zhang, J., Dodd, S.,

883 Nguyen-Trung, A.-T., Tian, H., Vogg, B., Beato, S., Garad, S., Choudhury, S., Ren, X., Mueller-

884 Zsigmondy, M., Einolf, H., Umehara, K., Hourcade-Potelleret, F., He, H., n.d. PBPK Modeling and

885 Simulations of Oral Drug Absorption/Food Effect/PPI /PBIVIVC: Opportunities and Challenges

886 Dissolution and Translational Modeling Strategies Enabling Patient-Centric Product

887 Development.

888 Heimbach, T., Suarez-Sharp, S., Kakhi, M., Holmstock, N., Olivares-Morales, A., Pepin, X., Sjögren, E.,

889 Tsakalozou, E., Seo, P., Li, M., Zhang, X., Lin, H.-P., Montague, T., Mitra, A., Morris, D., Patel, N.,

890 Kesisoglou, F., 2019. Dissolution and Translational Modeling Strategies Toward Establishing an

891 In Vitro-In Vivo Link—a Workshop Summary Report. AAPS J. 21, 29.

892 Hens, B., Brouwers, J., Anneveld, B., Corsetti, M., Symillides, M., Vertzoni, M., Reppas, C., Turner,

893 D.B., Augustijns, P., 2014. Gastrointestinal transfer: In vivo evaluation and implementation in in

894 vitro and in silico predictive tools. Eur. J. Pharm. Sci. 63, 233–242.

895 Jamei, M., Turner, D., Yang, J., Neuhoff, S., Polak, S., Rostami-Hodjegan, A., Tucker, G., 2009.

896 Population-based mechanistic prediction of oral drug absorption. AAPS J. 11, 225–237.

897 Kambayashi, A., Blume, H., Dressman, J., 2013. Understanding the in vivo performance of enteric

898 coated tablets using an in vitro-in silico-in vivo approach: Case example diclofenac. Eur. J.

899 Pharm. Biopharm. 85, 1337–1347.

900 Ke, A., Barter, Z., Rowland-Yeo, K., Almond, L., 2016. Towards a Best Practice Approach in PBPK

901 Modeling: Case Example of Developing a Unified Efavirenz Model Accounting for Induction of

902 CYPs 3A4 and 2B6. CPT Pharmacometrics Syst. Pharmacol. 5, 367–376.

903 Kuepfer, L., Niederalt, C., Wendl, T., Schlender, J.-F., Willmann, S., Lippert, J., Block, M., Eissing, T.,

904 Teutonico, D., 2016. Applied Concepts in PBPK Modeling: How to Build a PBPK/PD Model. CPT

905 pharmacometrics Syst. Pharmacol. 5, 516–531.

906 Lartigue, S., Bizais, Y., Des Varannes, S.B., Murat, A., Pouliquen, B., Galmiche, J.P., 1994. Inter- and

907   intrasubject variability of solid and liquid gastric emptying parameters. A scintigraphic study in

908   healthy subjects and diabetic patients. Dig. Dis. Sci. 39, 109–15.

909   Lennernas, H., Knutson, L., Knutson, T., Lesko, L., Salmonson, T., Amidon, G.L., 1995. Human effective

910   permeability data for furosemide, hydrochlorothiazide, ketoprofen and naproxen to be used in

911   the proposed biopharmaceutical classification for IR-products. Pharm. Res. (New York) 12(9

912   SUPPL) 396.

913   Lin, J.H., Cocchetto, D.M., Duggan, D.E., 1987. Protein binding as a primary determinant of the clinical

914   pharmacokinetic properties of non-steroidal anti-inflammatory drugs. Clin. Pharmacokinet. 12,

915   402–432.

916   Loisios-Konstantinidis, I., Paraiso, R.L.M., Fotaki, N., McAllister, M., Cristofoletti, R., Dressman, J.,

917   2019. Application of the relationship between pharmacokinetics and pharmacodynamics in drug

918   development and therapeutic equivalence: a PEARRL review. J. Pharm. Pharmacol. 71, 699–723.

919   Mann, J., Dressman, J., Rosenblatt, K., Ashworth, L., Muenster, U., Frank, K., Hutchins, P., Williams, J.,

920   Klumpp, L., Wielockx, K., Berben, P., Augustijns, P., Holm, R., Hofmann, M., Patel, S., Beato, S.,

921   Ojala, K., Tomaszewska, I., Bruel, J.-L., Butler, J., 2017. Validation of Dissolution Testing with

922   Biorelevant Media: An OrBiTo Study. Mol. Pharm. 14, 4192–4201.

923   Markopoulos, C., Andreas, C.J., Vertzoni, M., Dressman, J., Reppas, C., 2015. In-vitro simulation of

924   luminal conditions for evaluation of performance of oral drug products: Choosing the

925   appropriate test media. Eur. J. Pharm. Biopharm. 93, 173–182.

926   McNamara, D.P., Amidon, G.L., 1986. Dissolution of acidic and basic compounds from the rotating

927   disk: Influence of convective diffusion and reaction. J. Pharm. Sci. 75, 858–868.

928   Mitra, A., 2019. Maximizing the Role of Physiologically Based Oral Absorption Modeling in Generic

929   Drug Development. Clin. Pharmacol. Ther. 105, 307–309.

930 Mooney, K. G., Mintun, M.A., Himmelstein, K.J., Stella, V.J., 1981. Dissolution kinetics of carboxylic

931   acids I: Effect of pH under unbuffered conditions. J. Pharm. Sci. 70, 13–22.

932 Mooney, K.G., Mintun, M.A., Himmelstein, K.J., Stella, V.J., 1981a. Dissolution Kinetics of Carboxylic

933   Acids II: Effect of Buffers. J. Pharm. Sci. 70, 22–32.

934 Mooney, K.G., Rodriguez-gaxiola, M., Mintun, M., Himmelstein, K.J., Stella, V.J., 1981b. Dissolution

935   Kinetics of Phenylbutazone. J. Pharm. Sci. 70, 1358–1365.

936 Niazi, S.K., Mahmood Alam, S., Ahmad, S.I., 1996. Dose dependent pharmacokinetics of naproxen in

937   man. Biopharm. Drug Dispos. 17, 355–361.

938 Obach, R.S., Baxter, J.G., Liston, T.E., Silber, B.M., Jones, B.C., MacIntyre, F., Rance, D.J., Wastall, P.,

939   1997. The prediction of human pharmacokinetic parameters from preclinical and in vitro

940   metabolism data. J. Pharmacol. Exp. Ther. 283, 46–58.

941 Olivares-Morales, A., Ghosh, A., Aarons, L., Rostami-Hodjegan, A., 2016. Development of a Novel

942   Simplified PBPK Absorption Model to Explain the Higher Relative Bioavailability of the OROS®

943   Formulation of Oxybutynin. AAPS J. 18, 1532–1549.

944 Ozturk, S.S., Palsson, B.O., Dressman, J.B., 1988. Dissolution of Ionizable Drugs in Buffered and

945   Unbuffered Solutions. Pharm. Res. 05, 272–282.

946 Paixão, P., Bermejo, M., Hens, B., Tsume, Y., Dickens, J., Shedden, K., Salehi, N., Koenigsknecht, M.J.,

947   Baker, J.R., Hasler, W.L., Lionberger, R., Fan, J., Wysocki, J., Wen, B., Lee, A., Frances, A.,

948   Amidon, G.E., Yu, A., Benninghoff, G., Löbenberg, R., Talattof, A., Sun, D., Amidon, G.L., 2018.

949   Gastric emptying and intestinal appearance of nonabsorbable drugs phenol red and

950   paromomycin in human subjects: A multi-compartment stomach approach. Eur. J. Pharm.

951   Biopharm. 129, 162–174.

952 Paixão, P., Gouveia, L.F., Morais, J.A.G., 2012. Prediction of the human oral bioavailability by using in

953   vitro and in silico drug related parameters in a physiologically based absorption model. Int. J.

954   Pharm. 429, 84–98.

955   Parrott, N., Hainzl, D., Scheubel, E., Krimmer, S., Boetsch, C., Guerini, E., Martin-Facklam, M., 2014.

956   Physiologically Based Absorption Modelling to Predict the Impact of Drug Properties on

957   Pharmacokinetics of Bitopertin. AAPS J. 16, 1077–1084.

958   Pathak, S.M., Patel, N., Wedagedera, J., Turner, D.B., Jamei, M., Rostami-Hodjegan, A., Limited, S.,

959   1997. Establishment of Virtual Bioequivalence Using Population-Based PBPK Modelling:

960   Application to the Setting of Dissolution Limits, AAPS J.

961   Pathak, S.M., Schaefer, K.J., Jamei, M., Turner, D.B., 2019. Biopharmaceutic IVIVE—Mechanistic

962   Modeling of Single- and Two-Phase In Vitro Experiments to Obtain Drug-Specific Parameters for

963   Incorporation Into PBPK Models. J. Pharm. Sci. 108, 1604–1618.

964   Pepin, X.J.H., Flanagan, T.R., Holt, D.J., Eidelman, A., Treacy, D., Rowlings, C.E., 2016. Justification of

965   Drug Product Dissolution Rate and Drug Substance Particle Size Specifications Based on

966   Absorption PBPK Modeling for Lesinurad Immediate Release Tablets.

967   Pérez, M.A.C., Sanz, M.B., Torres, L.R., Évalos, R.G., González, M.P., Díaz, H.G., 2004. A topological

968   sub-structural approach for predicting human intestinal absorption of drugs. Eur. J. Med. Chem.

969   39, 905–916.

970   Petring, O.U., Flachs, H., 1990. Inter- and intrasubject variability of gastric emptying in healthy

971   volunteers measured by scintigraphy and paracetamol absorption. Br. J. Clin. Pharmacol. 29,

972   703–8.

973   Poulin, P., Theil, F.-P., 2009. Development of a novel method for predicting human volume of

974   distribution at steady-state of basic drugs and comparative assessment with existing methods.

975   J. Pharm. Sci. 98, 4941–4961.

976   Psachoulias, D., Vertzoni, M., Goumas, K., Kalioras, V., Beato, S., Butler, J., Reppas, C., 2011.

977   Precipitation in and Supersaturation of Contents of the Upper Small Intestine After

978   Administration of Two Weak Bases to Fasted Adults. Pharm. Res. 28, 3145–3158.

979   Rao, B.R., Rambhau, D., Rao, V.V.S., 1993. Pharmacokinetics of Single-Dose Administration of

980   Naproxen at 1O : OO and 22 : OO Hours. Int. Soc. Chronobiol. 10, 137–142.

981   Rosenberger, J., Butler, J., Muenster, U., Dressman, J., 2019. Application of a Refined Developability

982   Classification System. J. Pharm. Sci. 108, 1090–1100.

983   Runkel, R., Chaplin, M., Boost, G., Segre, E., Forchielli, E., 1972a. Absorption, Distribution,

984   Metabolism, and Excretion of Naproxen in Various Laboratory Animals and Human Subjects. J.

985   Pharm. Sci. 61, 703–708.

986   Runkel, R., Forchielli, E., Boost, G., Chaplin, M., Hill, R., Sevelius, H., Thompson, G., Segre, E., 1973.

987   Naproxen-metabolism, excretion and comparative pharmaco kinetics. Scand J Rheumatol. 2,

988   29–36.

989   Runkel, R., Karl, K., Boost, G., Sevilius, H., Forchielli, E., HILL, R., MAGOUN, R., SZAKACS, J.B., SEGRE,

990   E., 1972b. Naproxen Oral Absorption Characteristics. Chem. Pharm. Bull. (Tokyo). 20, 1457–

991   1466.

992   S. Darwich, A., Neuhoff, S., Jamei, M., Rostami-Hodjegan, A., 2010. Interplay of Metabolism and

993   Transport in Determining Oral Drug Absorption and Gut Wall Metabolism: A Simulation

994   Assessment Using the "Advanced Dissolution, Absorption, Metabolism (ADAM)" Model. Curr.

995   Drug Metab. 11, 716–729.

996   Selen, A., Dickinson, P.A., Müllertz, A., Crison, J.R., Mistry, H.B., Cruañes, M.T., Martinez, M.N.,

997   Lennernäs, H., Wigal, T.L., Swinney, D.C., Polli, J.E., Serajuddin, A.T.M., Cook, J.A., Dressman,

998   J.B., 2014. The biopharmaceutics risk assessment roadmap for optimizing clinical drug product

999   performance. J. Pharm. Sci. 103, 3377–3397.

1000   Serajuddin, A.T.M., Jarowski, C., 1985. Effect of diffusion layer pH and solubility on the dissolution

1001   rate of pharmaceutical bases and their hydrochloride salts. I: Phenazopyridine. J. Pharm. Sci. 74,

1002   142.

1003   Setiawati, E., Deniati, S., Yunaidi, D., Handayani, L., Harinanto, G., Santoso, I., Sari, P.A., Rimainar, A.,

1004   2009. Bioequivalence Study with Two Naproxen Sodium Tablet Formulations in Healthy

1005   Subjects. J. Bioequivalence Bioavailab. -Open Access Res. Artic. JBB J Bioequiv Availab 1, 28–33.

1006   Shebley, M., Sandhu, P., Emami Riedmaier, A., Jamei, M., Narayanan, R., Patel, A., Peters, S.A., Reddy,

1007   V.P., Zheng, M., de Zwart, L., Beneton, M., Bouzom, F., Chen, J., Chen, Y., Cleary, Y., Collins, C.,

1008   Dickinson, G.L., Djebli, N., Einolf, H.J., Gardner, I., Huth, F., Kazmi, F., Khalil, F., Lin, J., Odinecs,

1009   A., Patel, C., Rong, H., Schuck, E., Sharma, P., Wu, S.-P., Xu, Y., Yamazaki, S., Yoshida, K.,

1010   Rowland, M., 2018. Physiologically Based Pharmacokinetic Model Qualification and Reporting

1011   Procedures for Regulatory Submissions: A Consortium Perspective. Clin. Pharmacol. Ther. 104,

1012   88–110.

1013   Sheng, J.J., McNamara, D.P., Amidon, G.L., 2009. Toward an In Vivo dissolution methodology: A

1014   comparison of phosphate and bicarbonate buffers. Mol. Pharm. 6, 29–39.

1015   Stillhart, C., Parrott, N.J., Lindenberg, M., Chalus, P., Bentley, D., Szepes, A., 2017. Characterising Drug

1016   Release from Immediate-Release Formulations of a Poorly Soluble Compound, Basmisanil,

1017   Through Absorption Modelling and Dissolution Testing. AAPS J. 19, 827–836.

1018   Suarez-Sharp, S., Cohen, M., Kesisoglou, F., Abend, A., Marroum, P., Delvadia, P., Kotzagiorgis, E., Li,

1019   M., Nordmark, A., Bandi, N., Sjögren, E., Babiskin, A., Heimbach, T., Kijima, S., Mandula, H.,

1020   Raines, K., Seo, P., Zhang, X., 2018. Applications of Clinically Relevant Dissolution Testing:

1021   Workshop Summary Report. AAPS J. 20, 93.

1022   Tubic-Grozdanis, M., Bolger, M.B., Langguth, P., 2008. Application of Gastrointestinal Simulation for

1023   Extensions for Biowaivers of Highly Permeable Compounds. AAPS J. 10, 213–226.

1024   U.S.FDA Center for Drug Evaluation and Research (CDER), 2018a. Physiologically Based

1025   Pharmacokinetic Analyses — Format and Content Guidance for Industry.

1026   U.S.FDA Center for Drug Evaluation and Research (CDER), 2018b. Physiologically Based

1027   Pharmacokinetic Analyses — Format and Content Guidance for Industry.

1028   Upton, R., Williams, R., Kelly, J., Jones, R., 1984. Naproxen pharmacokinetics in the elderly. Br. J. Clin.

1029   Pharmacol. 18, 207–214.

1030   Van den Ouweland, F.A., Jansen, P.A., Tan, Y., Van de Putte, L.B., Van Ginneken, C.A., Gribnau, F.W.,

1031   1988. Pharmacokinetics of high-dosage naproxen in elderly patients. Int. J. Clin. Pharmacol.

1032   Ther. Toxicol. 26, 143–7.

1033   Vree, T.B., Van Den Biggelaar-Martea, M., Verwey-Van Wissen, C.P.W.G.M., Vree, J.B., Guelen, P.J.M.,

1034   1993. Pharmacokinetics of naproxen, its metabolite O-desmethylnaproxen, and their acyl

1035   glucuronides in humans. Biopharm. Drug Dispos. 14, 491–502.

1036   Wang, J., Flanagan, D.R., 2002. General solution for diffusion-controlled dissolution of spherical

1037   particles. 2. Evaluation of experimental data. J. Pharm. Sci. 91, 534–542.

1038   Wang, J., Flanagan, D.R., 1999. General solution for diffusion-controlled dissolution of spherical

1039   particles. 1. Theory. J. Pharm. Sci. 88, 731–738.

1040   Wedagedera, J., Cain, T., Pathak, S.M., Jamei, M., 2017. Virtual Bioequivalence Assessment of Two

1041   Tramadol Formulations using the Advanced Dissolution Absorption and Metabolism (ADAM)

1042   Model via Simcyp R Package.

1043   Yazdanian, M., Briggs, K., Jankovsky, C., Hawi, A., 2004. The "High Solubility" Definition of the Current

1044   FDA Guidance on Biopharmaceutical Classification System May Be Too Strict for Acidic Drugs.

1045   Pharm. Res. 21, 293–299.

1046   Zhang, X., Wen, H., Fan, J., Vince, B., Li, T., Gao, W., Kinjo, M., Brown, J., Sun, W., Jiang, W.,

1047 Lionberger, R., 2017. Integrating *In Vitro* , Modeling, and *In Vivo* Approaches to Investigate

1048 Warfarin Bioequivalence. CPT Pharmacometrics Syst. Pharmacol. 6, 523–531.

1049 Zhao, P., Rowland, M., Huang, S.-M., 2012. Best practice in the use of physiologically based

1050 pharmacokinetic modeling and simulation to address clinical pharmacology regulatory

1051 questions. Clin. Pharmacol. Ther. 92, 17–20.

1052 Zhao, Y., Le, J., Abraham, M., Hersey, A., Eddershaw, P., Luscombe, C., Butina, D., Beck, G.,

1053 Sherborne, B., Cooper, I., Platts, J., 2001. Evaluation of human intestinal absorption data and

1054 subsequent derivation of a quantitative structure-activity relationship (QSAR) with Abraham

1055 descriptors. J. Pharm. Sci. 90, 749–784.

1056 Zhou, D., Zhang, Q., Lu, W., Xia, Q., Wei, S., 1998. Single- and multiple-dose pharmacokinetic

1057 comparison of a sustained-release tablet and conventional tablets of naproxen in healthy

1058 volunteers. J. Clin. Pharmacol. 38, 625–629.

1059

1060

8 List of Figures

50

1132

1133

1134

1135

9 List of Tables

Table 1: Composition and physicochemical characteristics of biorelevant media in the fasted and fed states.

	Fasted state					Fed state			
	FaSSGF Level I	FaSSGF Level III	FaSSIF Level II	FaSSIF V3 Level I	FaSSIF V3 Level II	FeSSGF$_{middle}$ Level II	FeSSIF Level I	FeSSIF Level II	FeSSIF V2 Level II
Sodium Taurocholate (mM)	—	0.08	3.0	—	1,4	—	—	15	10
Sodium Glycocholate (mM)	—	—	—	—	1,4	—	—	—	—
Glyceryl monooleate (mM)	—	—	—	—	—	—	—	—	5
Sodium Oleate (mM)	—	—	—	—	0,315	—	—	—	0.8
Lecithin (mM)	—	0.02	0.75	—	0,035	—	—	3.75	2
Lysolecithin (mM)	—	—	—	—	0,315	—	—	—	—
Cholesterol (mM)	—	—	—	—	0,2	—	—	—	—
Pepsin (mg/mL)	—	0.1	—	—	—	—	—	—	—
Sodium dihydrogen phosphate (mM)	—	—	28.7	13,51	13,51	—	—	—	—
NaOH (mM)	—	—	13.8	3,19	3,19	—	101	101	102.4
Acetic acid (mM)	—	—	—	—	—	18.31	144	144	—
Maleic acid (mM)	—	—	—	—	—	—	—	—	71.9
Sodium acetate (mM)	—	—	—	—	—	32.98	—	—	—
Lipofundin®: buffer	—	—	—	—	—	8.75: 91.25	—	—	—
Hydrochloric acid	q.s. pH 1,6	q.s. pH 1,6	—	—	—	q.s. pH 5	—	—	—
Sodium chloride (mM)	—	34.2	106	—	91,62	181.7	—	204	125.5
Osmolality (mOsm/kg)	—	121	270	—	215	400	—	635	390
Buffer capacity (HCl) ((mmol/L)/ΔpH)	n.a.	n.a.	12	5,6	5,6	25	76	76	25
pH	1,6	1.6	6.5	6,7	6,7	5.0	5.0	5.0	5.8

q.s.- quantum satis; n.a.- not applicable

1170 *Table 2: Mean (SD) demographic data of in vivo studies used for the development and verification of the PBPK model. (HV= healthy*

1171 *volunteers)*

Reference	Formulation & Dose	N° of Subjects	Female Ratio	Ethnicity	Population	Age (y)	BW Range (kg)	BH Range (cm)
Intravenous								
(Runkel et al., 1973, 1972a, 1972b)	93 mg with 30µC tritium label in 100 mL phosphate buffer	3	0.33	Caucasian	HV	–	49.9-86.3	–
Oral								
(Charles and Mogg, 1994)	Naprosyn® 500 mg	16	0.125	Caucasian	HV	22.1 (4.4)	67.6 (8.3)	175.7 (9.0)
(Zhou et al., 1998)	Naprosyn® 2 x 250 mg	10	0	Chinese	HV	19-38	51-74	–
Haberer et al. (a)(Haberer et al., 2010)	Anaprox® 550 mg	8	0.63	Caucasian	HV	44.3 (8.5)	71.44 (12.3)	–
(Setiawati et al., 2009)	Anaprox® 550 mg	26	0.15	Caucasian	HV	19-46	–	–
(Rao et al., 1993)	IR Naproxen 500 mg	12	0	Indian	HV	18-22	46-62.5	160-182.5
Haberer et al. (b)(Haberer et al., 2010)	IR Naproxen-Na 500 mg	16	0.63	Caucasian	HV	44.3 (8.5)	71.44 (12.3)	–

1172

1173

1174

1175

Table 3: Input parameters for naproxen PBPK model development and simulations

Parameters	Value	Reference/ Comments
Physicochemical & Blood Binding		
MW (g/mol)	230.3	PubChem
$logP_{o:w}$	3.2	(Bergström et al., 2014; Pérez et al., 2004; Zhao et al., 2001)
pKa	4.43	estimated from *in vitro* data (see section 3.2)
Blood/ Plasma ratio	0.55	(Brown et al., 2007)
Fraction unbound in plasma	0.01	(Davies and Anderson, 1997; Paixão et al., 2012)
Absorption		
Model	ADAM	
$P_{eff, human}$ ($\times 10^{-4}$ cm/s)	8.5	(Lennernas et al., 1995)
Formulation type	Immediate Release	
In vivo dissolution	see Table 7,Table 8	estimated DLM scalars from *in vitro* data (see section 3.3.2)
S_0 (mg/mL)	0.0294	*in vitro* data (see section 3.1)
Particle density (g/mL)	1.20	Default value within ADAM
Particle size distribution	Monodispersed	Assumed as data not available
Particle radius (µm)	10	Default value within ADAM
$logK_{m:w}$ neutral	5.37	estimated from *in vitro* data (see section 3.2)
$logK_{m:w}$ ion	4.00	estimated from *in vitro* data (see section 3.2)
Distribution		
Model	Minimal PBPK with SAC	
V_{ss} (L/kg)	0.15	PE module

V_{sac} (L/kg)	0.075	PE module
Q_{sac} (L/h)	1.00	PE module
Elimination		
CL_{iv} (L/h)	0.40	PE module
CL_{renal} (L/h)	0.02	(Paixão et al., 2012)

1177

1178

1179

1180   *Table 4: Mean (± SD) equilibrium solubility in aqueous media at 37°C for 24h (Uniprep® method).*

	Naproxen		Naproxen Sodium	
Aqueous medium	pH_{final}	Solubility (µg/mL)	pH_{final}	Solubility (µg/mL)
Water	4.5	70.4 (1.2)	6.7	358.4 (18.1)
HCl acid (pH=1.2)	1.3	29.4 (6.4)	1.2	28.4 (0.72)
Acetate buffer (pH=4.5)	4.5	84.8 (4.2)	4.6	103.1 (3.6)
Level I FeSSIF V1 (pH=5.0)	5.0	175.4 (0.0202)	5.1	241.6 (5.2)
Phosphate buffer (pH=6.5)	6.2	1627.6 (31.5)	6.6	2363.4 (31.5)
Phosphate buffer(pH=6.8)	6.5	3619.1 (112.6)	6.9	4957 (119)
Phosphate buffer (pH=7.4)	6.8	5981.6 (28.0)	7.5	10128 (674)

1181

1182

1183   *Table 5: Mean (± SD) equilibrium solubility in fasted and fed state biorelevant media at 37°C for 24h (Uniprep® method).*

Biorelevant medium	Naproxen		Naproxen Sodium	
	pH_{final}	Solubility (µg/mL)	pH_{final}	Solubility (µg/mL)
Fasted state				
Level III FaSSGF (pH=1.6)	1.6	33.4 (1.1)	1.6	31.8 (0.92)
Level II FaSSIF V1 (pH=6.5)	5.9	2046 (150)	6.5	3587 (179)
Level II FaSSIF V3 (pH=6.7)	5.8	1624 (153)	6.7	3469 (187)
Fed state				
Level II FeSSGF$_{middle}$ (pH=5.0)	4.9	352.6 (21.4)	5.1	575.2 (19.3)
Level II FeSSIF V1 (pH=5.0)	5.0	424.7 (26.6)	5.0	519.9 (18.9)
Level II FeSSIF V2 (pH=5.8)	5.8	890.0 (56.7)	5.8	799.5 (177)

1184

1185

1186   *Table 6: Parameter estimates (95% CI) resulting from the model-based analysis of in vitro solubility data in aqueous as well as*

1187   *biorelevant media. The pka was estimated from the aqueous solubility values, whereas for the micelle-water partition*

1188   *coefficients (logK$_{m:w}$ neutral, ion) estimation, biorelevant solubilities were used. The accuracy of the predictions was evaluated*

1189   *with the R squared.*

	pKa	logK$_{m:w}$ neutral	logK$_{m:w}$ ion
Estimate (95% CI)	4.43 (4.42-4.44)	5.37 (5.34-5.40)	4.00 (3.98-4.02)
R^2	0.9990	0.9999	

1190

1191

1192

Dissolution Medium	API Powder	
	NPX	NPX Na
Level I FaSSIF V3		
DLM (95% CI)	0.0022 (0.0021-0.0023)	1*
R^2	0.997	–
Eur. Phar. Phosphate Buffer (pH=6.8)		
DLM (95% CI)	0.0136 (0.0121-0.0151)	1*
R^2	0.992	–
Level II FaSSIF V3		
DLM (95% CI)	0.0810 (0.0651-0.0970)	1*
R^2	0.998	–

* default values of DLM scalar due to very fast dissolution (>85% dissolved in 2.5 min)

1196

1197

Dissolution Medium	Formulation	
	Naprosyn	Anaprox
Level I FaSSIF V3		
DLM (95% CI)	0.0296 (0.0149-0.0443)	0.0212 (0.0131-0.0294)
kd (95% CI)	0.305 (0.123-0.487)	0.288 (0.130-0.446)
R^2	0.999	0.998
Level I FaSSIF V3 (two-stage)		
DLM (95% CI)	0.0305 (0.0191-0.0308)	0.0221 (0.0174-0.0267)
kd (95% CI)	–	–
R^2	0.967	0.981
Level II FaSSIF V3		
DLM (95% CI)	0.0213 (0.0170-0.0255)	0.0168 (0.00996-0.0237)
kd (95% CI)	0.702 (0.354-1.05)	0.228 (0.0975-0.358)
R^2	0.999	0.999
Level II FaSSIF V3 (two-stage)		
DLM (95% CI)	0.0187 (0.0143-0.0230)	0.0158 (0.0138-0.0179)
kd (95% CI)	–	–
R^2	0.975	0.991

1202

1203

Table 9: Mean in silico population pharmacokinetic (popPBPK) parameters of naproxen simulated plasma-concentration-time profiles under all tested in vivo dissolution inputs (DLM scalar values) as obtained from model-based analysis of the in vitro data (see formulation and dissolution medium).

Formulation	Medium	S_{DLM}	Disintegration	*In silico* mean popPBPK parameters		
			kd (h^{-1})/2-stage	t_{max} (h)	C_{max} (mg/L)	AUC (mg/L·h)
API						
Naproxen						
	Level I FaSSIF V3	0.0022	–	2.52	65.5	1302
	Ph. Eur. Phosphate	0.0136	–	1.80	69.0	1305
	Level II FaSSIF V3	0.0810	–	1.44	69.4	1306
Naproxen Na						
	all media	1	–	1.44	69.6	1306
Formulation						
Naprosyn						
	Level I FaSSIF V3	0.0396	0.305	1.80	67.5	1277
		0.0305	2-stage	1.80	69.2	1306
	Level II FaSSIF V3	0.0213	0.702	1.80	67.8	1277
		0.0187	2-stage	1.80	69.1	1306
Anaprox						
	Level I FaSSIF V3	0.0212	0.288	1.80	67.9	1277

	0.0221	2-stage	1.80	69.2	1306
Level II FaSSIF V3	0.0168	0.228	1.80	67.7	1277
	0.0158	2-stage	1.80	69.1	1305

1207

1208

1209   *Table 10: Mean (SD) pharmacokinetic parameters of naproxen in vivo studies (^{a} Median value).*

Reference	Formulation & Dose	In vivo mean PK parameters (SD)		
		t_{max} (h)	C_{max} (mg/L)	AUC (mg/L·h)
(Charles and Mogg, 1994)	Naprosyn® 500 mg	1.50[a]	71.4[a]	1211[a]
(Zhou et al., 1998)	Naprosyn® 2 x 250 mg	2.6 (1.5)	87.3 (15.5)	1428 (193)
(Haberer et al., 2010)	Anaprox® 550 mg	1.48	75.2	1294
(Setiawati et al., 2009)	Anaprox® 550 mg	1.00 (0.5-2)	72.0 (11.2)	1013 (186)
(Rao et al., 1993)	IR Naproxen 500 mg	1.36 (0.81)	69.2 (20.9)	1435 (312)
Haberer et al. (b)(Haberer et al., 2010)	IR Naproxen-Na 500 mg	1.53	74.9	1299

1210

1211

Table 11: Mean in silico population pharmacokinetic (popPBPK) parameters of naproxen virtual clinical trials for the

1213   *hypothetical reference and test formulations prior to bioequivalence assessment.*

Trial N°	In silico mean popPBPK parameters					
	Reference			Test		
	t_{max} (h)	C_{max} (mg/L)	AUC (mg/L·h)	t_{max} (h)	C_{max} (mg/L)	AUC (mg/L·h)
1	1.66	62.01	1249	2.26	57.66	1248
2	1.51	65.79	1275	2.31	62.58	1273
3	1.96	61.30	1624	2.59	59.67	1623
4	1.58	74.97	1659	2.41	70.61	1657
5	1.75	60.35	1785	2.84	55.14	1783
6	1.55	72.27	1404	2.56	67.34	1403
7	1.45	64.14	1426	2.02	62.17	1425
8	1.39	71.03	1473	2.47	65.14	1472
9	1.58	61.87	1340	2.26	58.88	1339
10	1.64	62.32	1348	2.39	60.46	1347

1214

1215

1216   Figure 1:

1217

1218
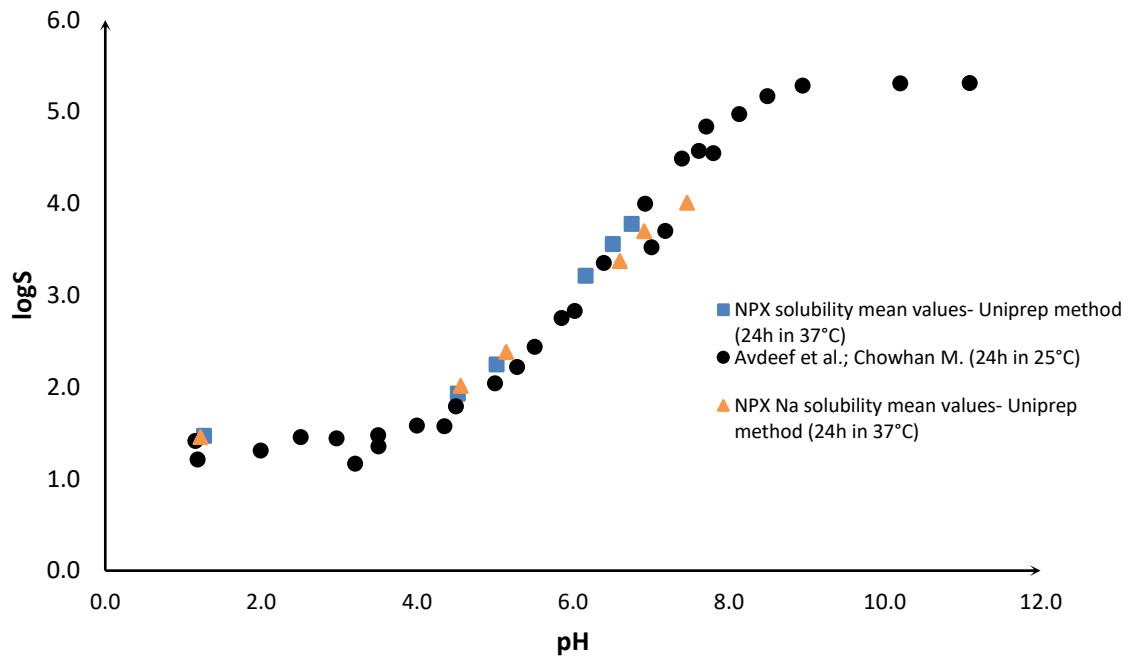
1219

1220   Figure 2:

1221

1222

1223

1224
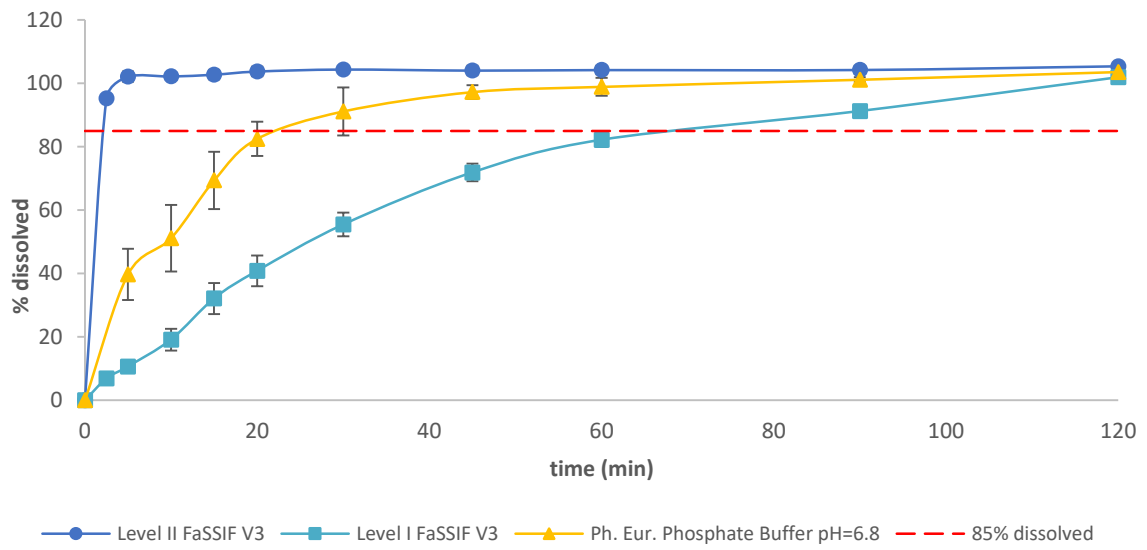
1225   Figure 3:

1226

1227
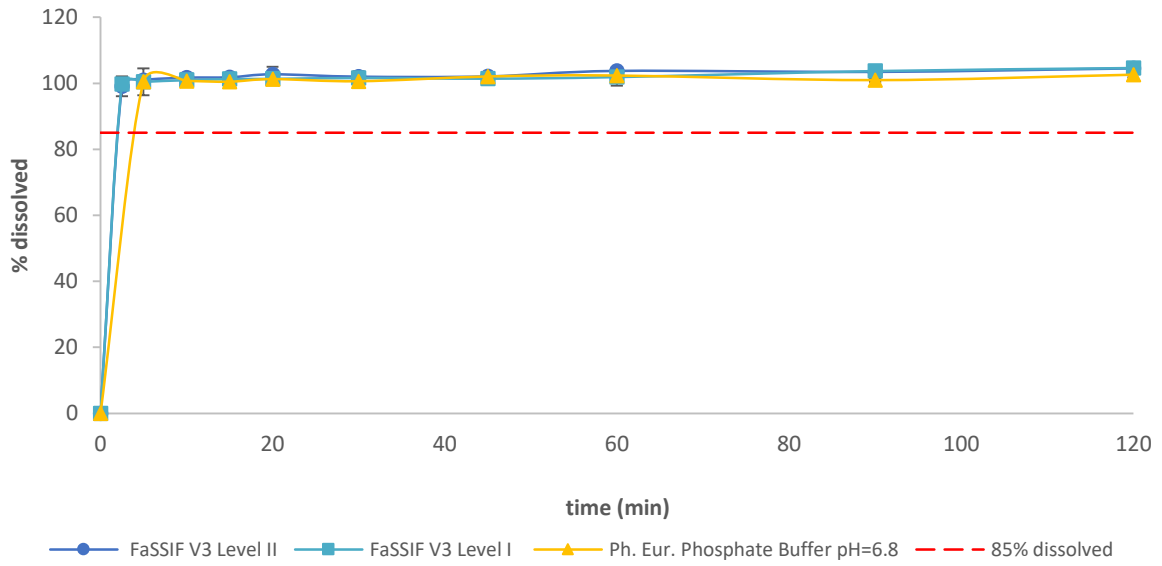
1228

1229   Figure 4:

1230
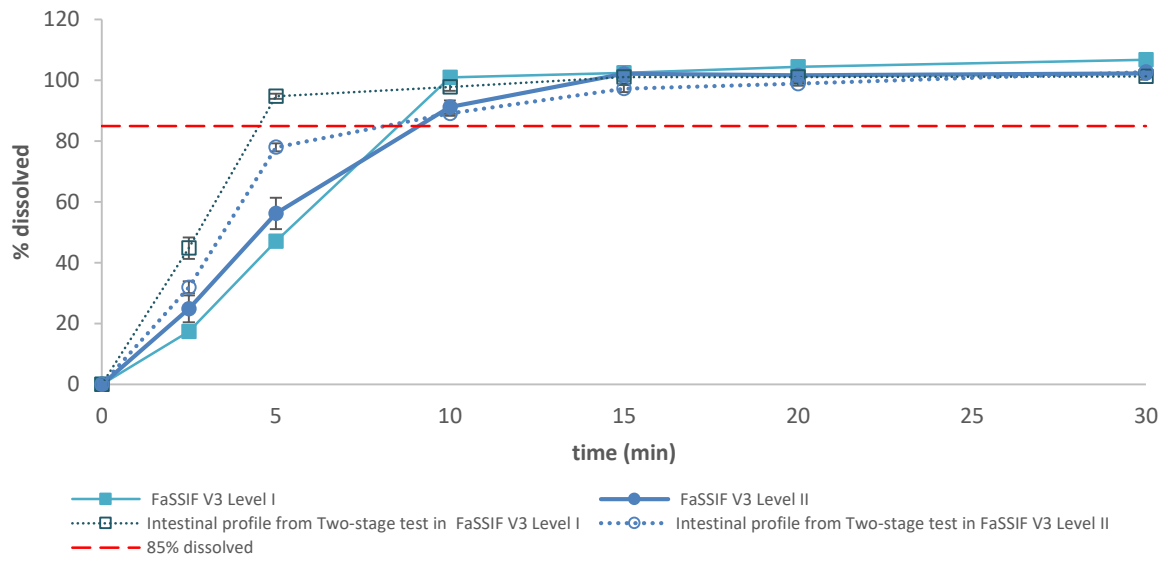
1231

1232

1233

1234   Figure 5:

1235
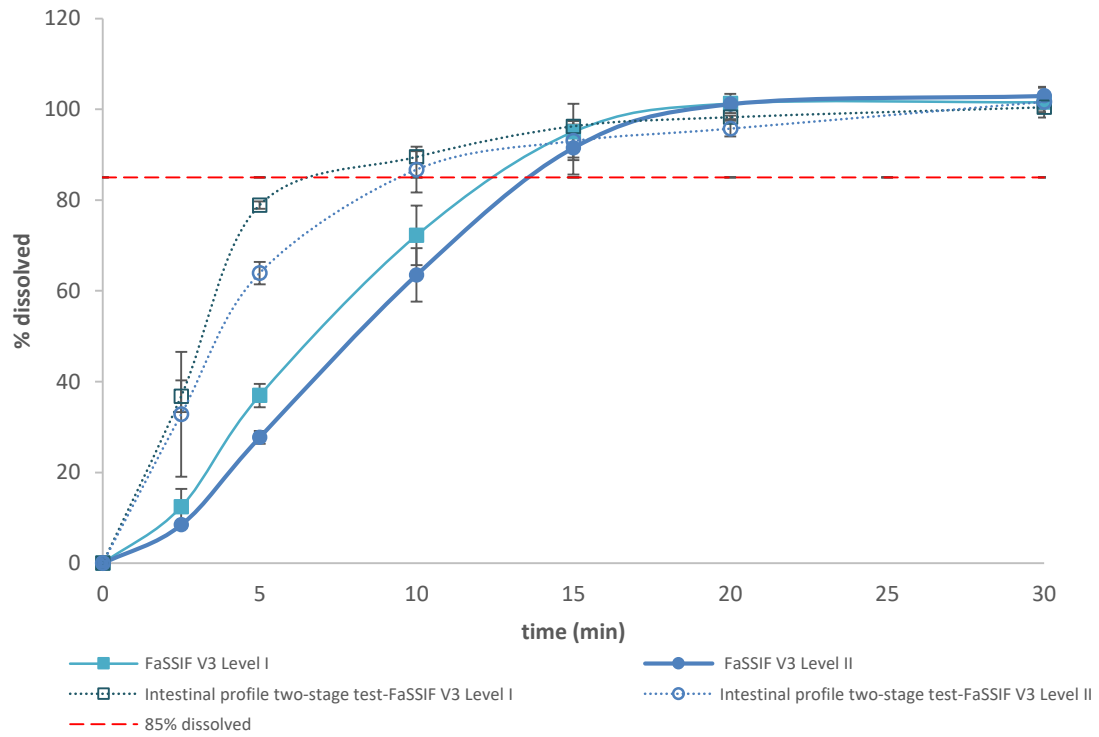
1236

1237

1238

1239   Figure 6:

1240

1241

1242

1243

1244
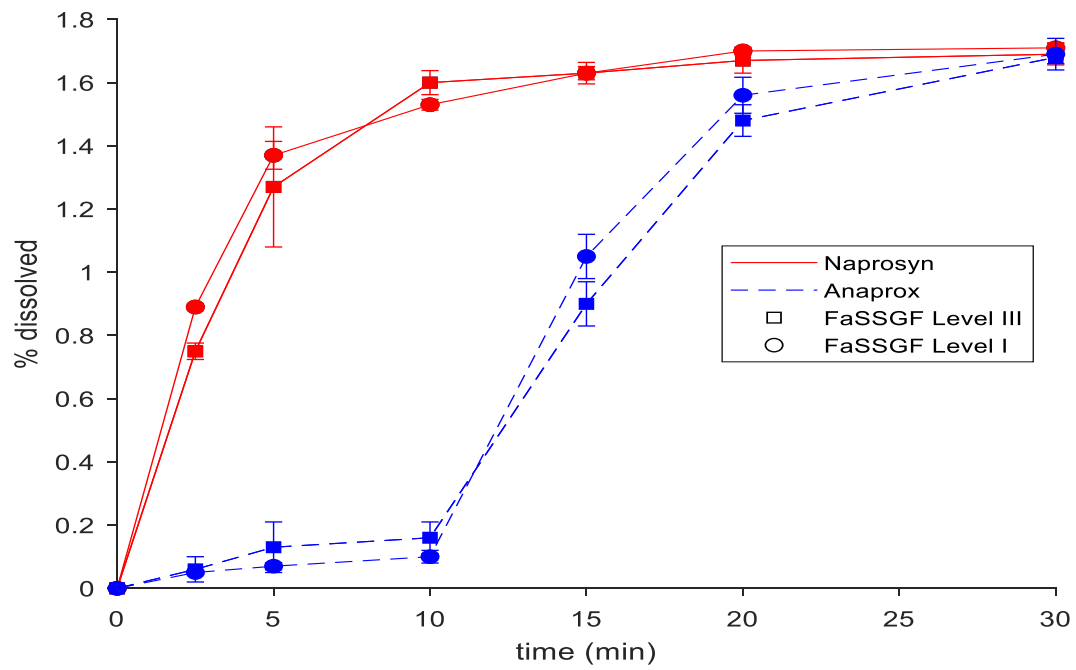
1245

1246

1247

1248   Figure 7:
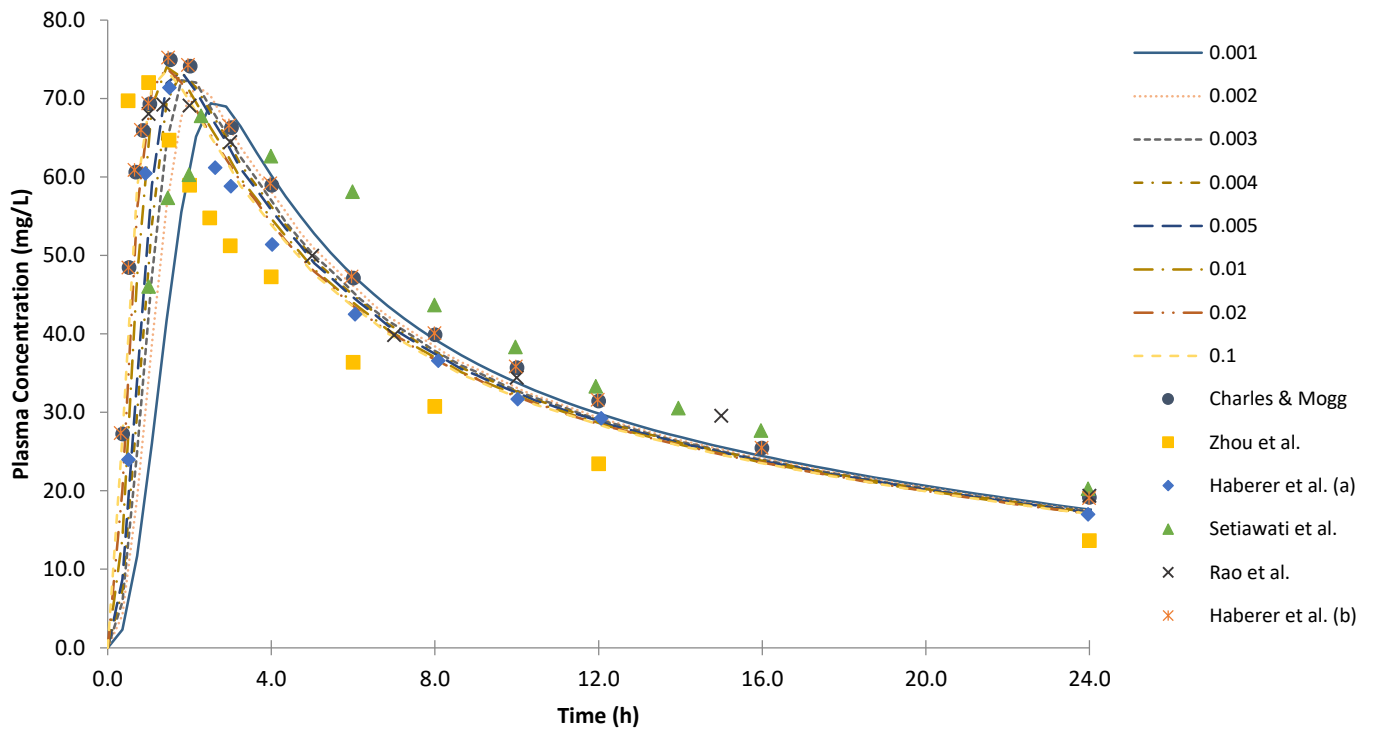
1249

1250
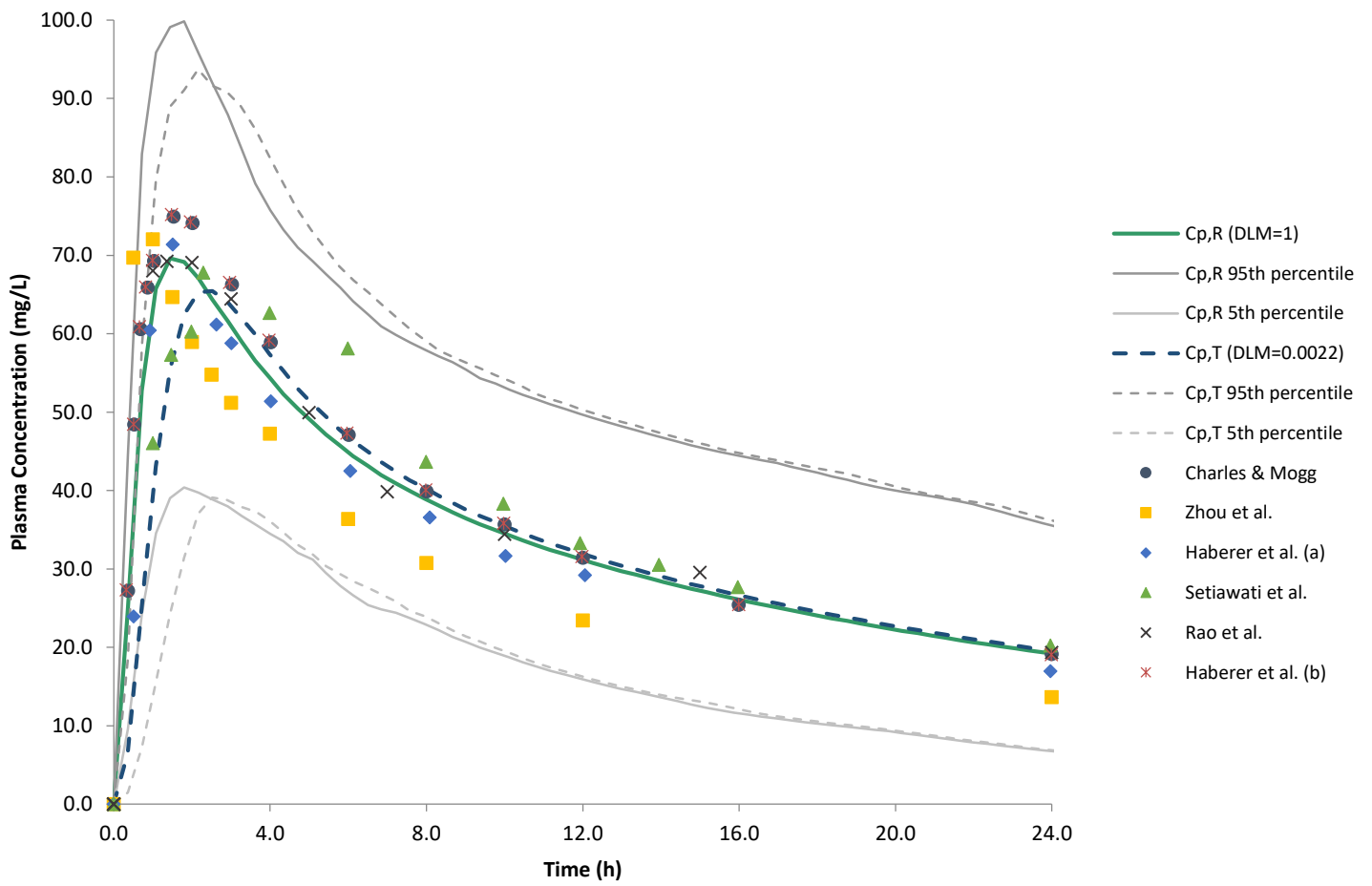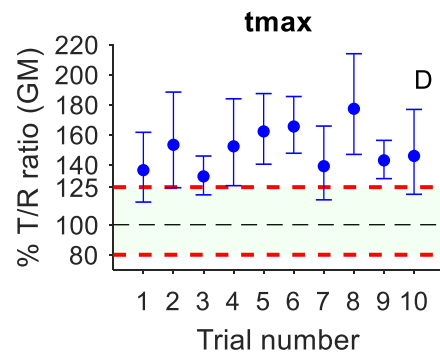

1251

1252

1253
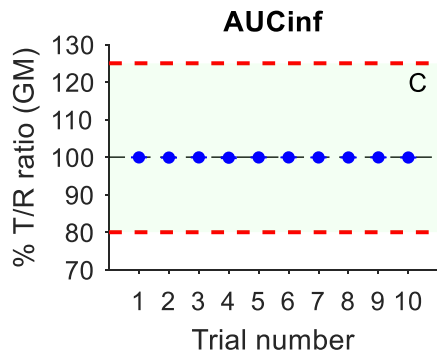
Figure 8:

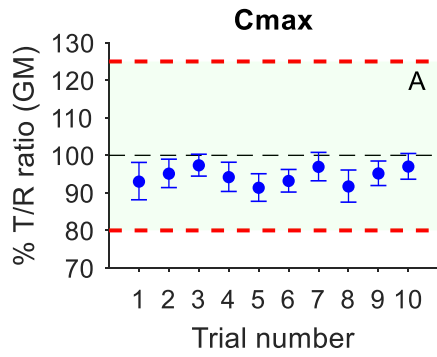1258   Figure 9:

1259

1260
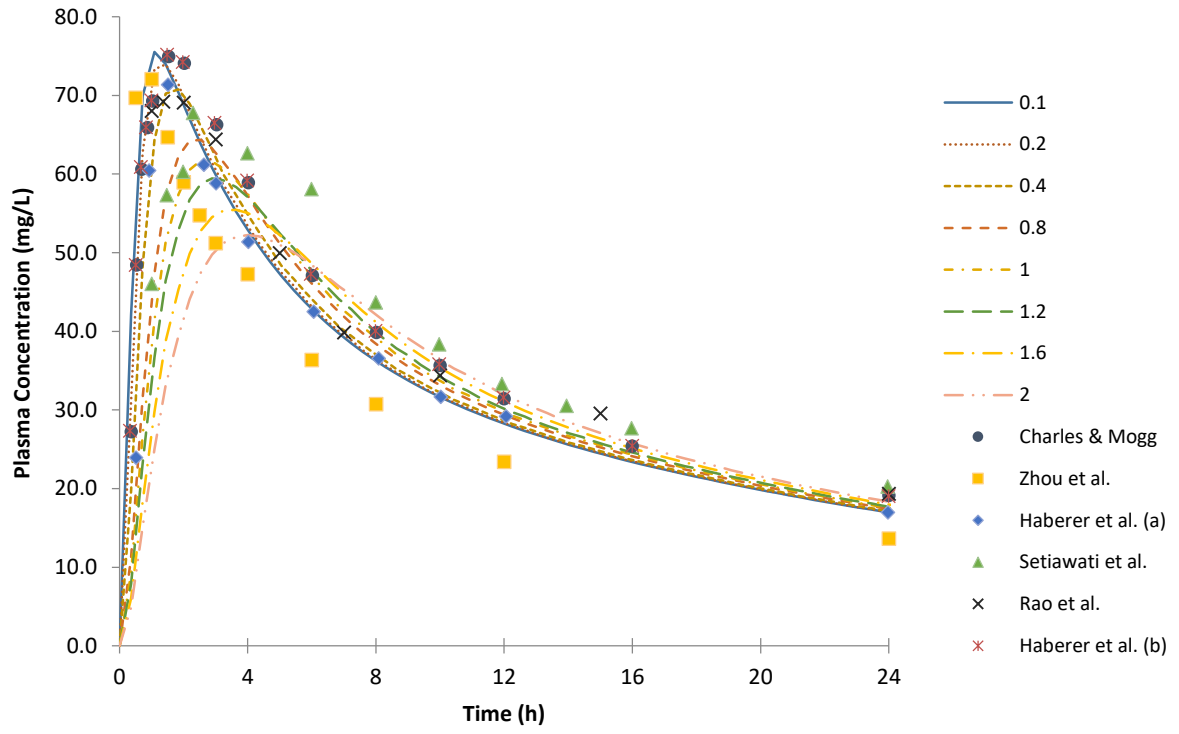
1261

1262

1263

1264   Figure 10:
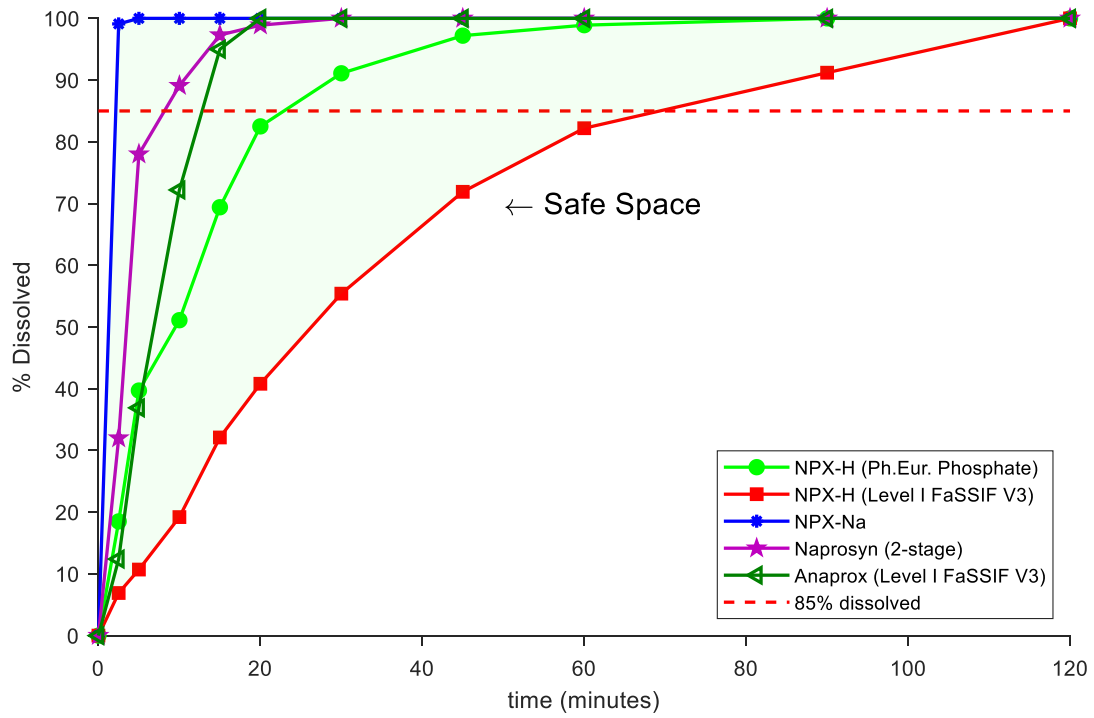
1265
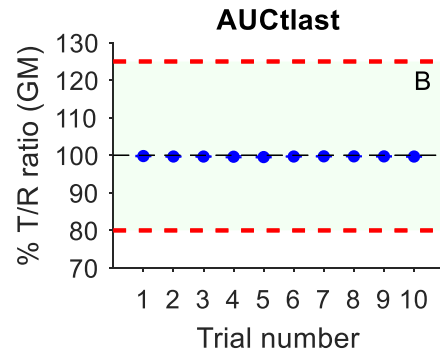
1266

1267

1268

1269

1270

1271

1272

1273

1274

1275

1276

1277

1278

1279

1280   Figure 11:

1281

1282